Finite-friction least-thickness self-standing domains of symmetric circular masonry arches. Part II: Milankovitch-like self-weight distribution

Giuseppe COCCHETTI [1,2], Egidio RIZZI [2,*]

[1]Politecnico di Milano, Dipartimento di Ingegneria Civile e Ambientale,
piazza Leonardo da Vinci 32, I-20133 MILANO, Italy

[2]Università degli studi di Bergamo, Dipartimento di Ingegneria e Scienze Applicate,
viale Guglielmo Marconi 5, I-24044 DALMINE (BG), Italy

[*]Corresponding Author: egidio.rizzi@unibg.it

Accepted Preprint: 25 March 2025

Abstract

The present paper constitutes a sort of compendium to a recent analysis considering the role of finite (Coulomb) friction in the mechanics of (symmetric circular) masonry arches, toward addressing least-thickness self-standing states and collapse modes possibly including sliding. Thereby, a classical Heyman-like uniform self-weight distribution along geometrical centre-line was considered, and all characteristic features delivered, by a comprehensive analytical approach, corroborated by consistent outcomes from a self-made numerical Complementarity Problem/Mathematical Programming implementation. The same is now updated, for the real Milankovitch-like uniform self-weight distribution, considering the true positions of the centres of gravity of the ideal wedged-shaped chunks of the arch, with radial stereotomy. The main achieved result is that the specific conceived distribution does not alter, conceptually, the salient recorded characteristic features, in terms of types of self-standing/collapse states, though some differences are displayed, in the details of the final analytical-numerical findings, with few physical implications. However, the main implant, put to light from the previous, simpler to be mathematically handled, classical self-weight distribution, is confirmed, showing definite reference, in methodological terms, discovered features and first-order amount of technical results. In general sense, the present true Milankovitch-like self-weight distribution leads to more precise results, which support further bearing capacity for the real arch, thus anyway with conservative estimates arising from the previous approximate Heyman-like self-weight distribution, quite simpler in the underlying mechanical and mathematical treatment.

Keywords: (symmetric circular) masonry arches; Couplet-Heyman problem; least thickness; collapse modes; finite friction; Milankovitch-like self-weight distribution.

1 Introduction

The present paper concerns the classical "Couplet-Heyman problem" of self-standing least-thickness (symmetric circular) masonry arch optimization, in the wake of cornerstone formulations by Milankovitch [1] and Heyman [2], but in the attempt to highlight the role that finite friction may display in possibly leading to collapse modes including sliding (thus releasing third classical Heyman hypothesis of no sliding failure).

This has recently been investigated, on a comprehensive analytical basis, with an associated numerical validation and illustration by a Complementarity Problem/Mathematical Programming (CP/MP) implementation, in paper [3], which constitutes the source of this companion work, whereby a classical Heyman-like uniform self-weight distribution along geometrical centreline of the arch was considered. Here, the same is then pursued for the real Milankovitch-like self-weight distribution, accounting for the true positioning of the centres of gravity of the ideal, wedge-shaped, radial-joint chunks of the continuous arch. Possible differences, in general conceptual terms, and technical details, among the outcomes linked to the two self-weight distributions are sought, specifically in the above-stated terms of deciphering finite-friction effects.

Previous work [3] here constitutes a main reference, and the present technical description forms a sort of synthetic compendium of what has been derived there. Similarly, as per a wide reference framing within the pertinent literature, the interested reader may be sent to that, for possible inspection and deepening. Of further specific support may instead be earlier works [4–9], within which this investigation by the present Authors is set, also in terms of basic concepts and underlying adopted notation, and particular outcomes, as selectively cited as needed in the sequel, especially toward possible independent replication of the present analytical treatment, and derived "exact" solution. Particularly, direct comparisons, among the implications of the two self-weight distributions, concerning purely-rotational collapse modes, were earlier reported in [4, 8, 9], which also constitute a first immediate reference, in terms of mutual positioning among Milankovitch-like and Heyman-like self-weight distributions, and resulting mechanical implications. Additional literature contextualization, specifically pertinent to the issue of finite friction, is further introduced and discussed in the Conclusions.

Presentation follows the same structure adopted in [3], to provide addendum. Subsequent Section 2 presents the basic underlying mechanical equations, by addressing the role of the two assumed uniform self-weight distributions, in the description of the rotational activation of failure joints; moreover, a full picture of all the modes involving pure rotation is then innovatively achieved. Section 3 delivers further main outcomes, in the coupling to finite-friction effects, for the newly considered Milankovitch-like distribution, with direct comparison to the previous results for the Heyman-like distribution. Section 4 accordingly portrays landmark arch states and collapse modes, through the above-mentioned, adapted, CP/MP numerical formulation, for illustration and validation purposes. Closing Section 5 outlines several salient general and specific remarks out of the present analytical and numerical analysis on the Mechanics of (symmetric circular) masonry arches, in methodological and physical terms.

2 Underlying relations and analytical treatment

The governing equations for a consistent description of the Mechanics of self-standing/collapsing (symmetric circular) continuous masonry arches shall express a (correct) Heyman-like treatment of purely-rotational collapse [4, 8, 9], at undefined (high or infinite) friction, accounting for either Heyman-like or Milankovitch-like uniform self-weight distribution, and then introduce the account of finite friction [6] (here interpreted through Coulomb friction coefficient $\mu = \tan\varphi$, or friction angle $\varphi = \arctan\mu$), for investigating a possible sliding onset (disregarding for the specific assumed self-weight distribution, influencing the positioning of the self-weight resultants, not of the resultants themselves).

This is outlined below [3], in terms of typical circular masonry arch characteristics (Fig. 1):

$$\beta = \beta_{r,s} \ , \quad \eta = \frac{t}{r} \ , \quad h = \frac{H}{wr} \quad (w = \gamma \, t \, d) \tag{1}$$

where β is the angular inner-joint position from the crown ($0 \leq \beta \leq \alpha$, α half-opening angle of the symmetric circular arch), either rotational, $\beta = \beta_r$, or sliding, $\beta = \beta_s$, η is the thickness-to-radius ratio, whereby r and t are the radius and thickness of the circular masonry arch, while d is its out-of-plane depth, and h is the non-dimensional horizontal thrust, whereby H is the horizontal thrust and γ and w are the specific weights per unit volume and per unit length of geometrical centreline of the arch (alternatively, intrinsic non-dimensional horizontal thrust $\hat{h} = \eta h = H/[\gamma d r^2]$, at given physical arch characteristics γ, d, r).

Figure 1.

2.1 Rotational joint failure activation (at high-enough or infinite friction)

The governing equations for rotational activation [3] are modified, from Heyman-like uniform self-weight distribution, since resultants' positioning is affected, by Milankovitch-like uniform self-weight distribution (Fig. 1). They can be expressed as follows [4, 8, 9]:

- Relative rotational equilibrium relation of the upper or lower portion of the half-arch (under symmetry conditions), with respect to the inner intrados hinge at the haunch at angular position $\beta = \beta_r$ from the crown ($h_1 = h_L$ "Lower thrust", equilibrium from above; h_U "Upper thrust", equilibrium from below, see [10], to be derived for Milankovitch-like uniform self-weight distribution as in [8]):

$$h = h_1 = h_L(\beta, \eta) = \frac{(2-\eta)\beta \sin\beta - 2(1-\cos\beta) \, fac_M}{2 + \eta - (2-\eta)\cos\beta} \tag{2}$$

or

$$h = h_U(\alpha, \beta, \eta) = \frac{(2+\eta)\alpha \sin\alpha - (2-\eta)\beta \sin\beta - 2(\cos\beta - \cos\alpha) \, fac_M}{(2-\eta)\cos\beta - (2+\eta)\cos\alpha} \tag{3}$$

- Absolute rotational equilibrium relation of the whole half-arch, with respect to the extrados hinge at the shoulder, involving a dependence on half-opening angle α, only through variable $A(\alpha) = \alpha \cot(\alpha/2)$:

$$h = h_2(\alpha, \eta) = A(\alpha) - \frac{2}{2+\eta} \, fac_M \ , \quad A(\alpha) = \frac{\alpha \sin\alpha}{1 - \cos\alpha} = \alpha \cot\frac{\alpha}{2} \tag{4}$$

- Limit tangency condition of the line of thrust (locus of pressure points) at the haunch intrados in the least-thickness condition (updated from single term h_H characteristic of classical "approximate" Heyman solution [2], holding for η small):

$$h = h_e(\beta, \eta) = \underbrace{\beta \cot\beta}_{h_H} + 1 - \frac{2}{2-\eta} \, fac_M = \underbrace{\beta \cot\beta}_{h_H} - \frac{\eta}{2-\eta} \left(1 + \frac{2}{\eta} \left(fac_M - 1 \right) \right) \tag{5}$$

In the above relations, Milankovitch-like real uniform self-weight distribution factor fac_M, accounting for the true location of the centres of gravity of each theoretical infinitesimal chunk of the continuous arch, at radial distance $r_G = r\,(1+\eta^2/12)$, see Fig. 1, may be enabled, through on/off control flag δ_M ($\delta_M = 1/0$), with respect to classical Heyman-like uniform self-weight distribution along geometrical centreline ($\delta_M = 0$), as follows:

$$fac_M = \left(1 + \delta_M \;\eta^2/\,12\right) \tag{6}$$

with $fac_M \geq 1$, $(fac_M - 1) = \delta_M\,\eta^2/12 \geq 0$, which, for $\delta_M = 1$, clearly brings in further non-linear dependence on η, to be increasingly appreciated, at growing non-small η, while $fac_M = 1$, $(fac_M - 1) = 0$, for $\delta_M = 0$.

For Milankovitch-like uniform self-weight distribution ($\delta_M = 1$), the corresponding **purely-rotational solution** can be derived in explicit analytical form, out of the following *"cubic algebraic problem"*, in classical rotational triplet $A(\beta)$, $\eta(\beta)$, $h(\beta)$ ($\beta = \beta_r$) [4,9]:

$$\begin{cases} pol_A^M = S^2(3g-2S)\,A^3 + 3gS(g-f)\,A^2 - 3fg^2\,A + 2g^3 = 0; \\ pol_\eta^M = S\,\eta^3 + 3(f+g)\,\eta^2 - 12(g-S)\,\eta + 12(g-f) = 0; \\ pol_h^M = 6S^2\,h^3 - 3S(3f-g-2S)\,h^2 - 3(g-f)(f-2S)\,h + 2(g-f)^2 = 0. \end{cases} \tag{7}$$

where

$$\begin{aligned} &f = (\beta S)' = S + \beta C, \qquad g = fC + \beta S^2 = \beta + SC; \\ &S = \sin\beta\,,\; C = \cos\beta; \quad \text{with link} \;\; \beta S^2 + Cf - g = 0 \end{aligned} \tag{8}$$

and symbol $'$ denotes first-order differentiation with respect to angular position β.

The arising purely-rotational solution can be obtained by the two-branched explicit analytical solution of third-order Eqs. (7), as follows (two meaningful real-valued branches; same sign, either $+$ or $-$ in the two terms where $\pm$ appears, i.e. $+,+$ or $-,-$, or $\mp$ appears, i.e. $-,-$ or $+,+$, in the given order) [9]:

$$\begin{aligned} A_M = &\frac{g}{S(3g-2S)}\Bigg(-(g-f)+ \\ &\left(\frac{1\pm \mathrm{i}\sqrt{3}}{2^{2/3}}\right)\frac{(f+g)^2 - f(g+2\,S)}{\Big((g-f)\big(2(f+g)^2 + f(g-6S)\big) + 2S(3g-2S)^2 + (3g-2S)\;SQRT\Big)^{1/3}} + \\ &\left(\frac{2^{2/3}}{1\pm \mathrm{i}\sqrt{3}}\right)\Big((g-f)\big(2(f+g)^2 + f(g-6S)\big) + 2S(3g-2S)^2 + (3g-2S)\;SQRT\Big)^{1/3}\Bigg) \end{aligned} \tag{9}$$

$$\begin{aligned} \eta_M = &\frac{1}{S}\Bigg(-(f+g)+ \\ &\left(\frac{1\mp \mathrm{i}\sqrt{3}}{2}\right)\frac{(f+g)^2 + 4S(g-S)}{\Big((f+g)^3 + 6gS(f+g) - 12fS^2 + 2S\;SQRT\Big)^{1/3}} + \\ &\left(\frac{2}{1\mp \mathrm{i}\sqrt{3}}\right)\Big((f+g)^3 + 6gS(f+g) - 12fS^2 + 2S\;SQRT\Big)^{1/3}\Bigg) \end{aligned} \tag{10}$$

$$h_M = \frac{1}{6S}\Bigg(3f - g - 2S + \left(\frac{1 \pm \mathrm{i}\sqrt{3}}{2}\right)\frac{3f^2 + g^2 - 4S(2g - S)}{\Big(-g\,(9f^2 - g^2) - 2S\big(9f(g - f) - 12g(g - S) - 4S^2\big) + 3(g - f)\;SQRT\Big)^{1/3}} + \left(\frac{2}{1 \pm \mathrm{i}\sqrt{3}}\right)\Big(-g\,(9f^2 - g^2) - 2S\big(9f(g - f) - 12g(g - S) - 4S^2\big) + 3(g - f)\;SQRT\Big)^{1/3}\Bigg) \tag{11}$$

with

$$SQRT = \sqrt{9S^2(g - f)^2 - 2S(g - S)\,(9f^2 - g^2 - 16gS + 8S^2) - 3(f + g)^2\,(f^2 - 2gS + S^2)} \tag{12}$$

where i is the imaginary unit and the term under square root in Eq. (12) is negative in the β-range of interest, until it vanishes at $\beta^M_{s\beta} = 1.119864231443752 \simeq 64.2°$, corresponding to the stationary condition with widest angular inner hinge position for the purely-rotational collapse mode (at $\alpha = \alpha^M_{s\beta} = 2.196404448812124 \simeq 125.8°$), assuring real-valued solution branches [4, 9].

Clearly, the achieved analytical explicit two-branched purely-rotational solution (in terms of variable A) is much complex, than for the case of Heyman-like distribution [3, 4, 8, 9]. Moreover, differences are rather limited in the resulting purely-rotational outcomes. Indeed, the purely-rotational solutions are reported in the analytical-numerical plots depicted in Fig. 2, for classical Heyman-like triplet $\beta = \beta_r, \eta, h$, as a final function of α, whereby a numerical rooting is necessary just to resolve transcendental equation $A(\alpha) = \alpha \cot(\alpha/2)$. Specifically, some differences may be seen for angular position $\beta = \beta_r$ of the inner rotational joint, playing as a sort of internal ingredient, in the formulation, especially in a kind of "overshooting" of the Heyman-like solution around and after the peak of the $\beta_r(\alpha)$ curve (extremal condition analytically investigated in [9]), while differences in external variables η and h are really minimal, amazingly even at increasing least-thickness ratio η, but in particular in (usual) α-ranges whereby η is led to keep small.

Figure 2.

Milankovitch-like purely-rotational solution holds true until limit $\alpha^M_l = 2.590843443008955 \simeq 148.4°$, where $\beta = \beta_r$ pulls back to 0, reaching $h = 0$, at $\eta^M_l = 2(2\sqrt{3} - 3) = 0.9282032302755092$, i.e. at nearly 0.93, shifting (continuously) to a purely-overturning mode of the half-arch, with respect to the extrados hinge at the shoulder, while, for Heyman-like self-weight distribution, such limit values are slightly higher, namely $\alpha^H_l = 2.648388899151005 \simeq 151.7°$ and $\eta^H_l = 1$, thus, for both, with α_l say around 150°, at η_l near 1.

Indeed, this analytically comes from condition $h_2 = 0$, from Eq. (4) (or from condition $h_U|_{\beta_r = 0} = 0$, from Eq. (3), namely the other rotational relation containing α), leading to

$$A(\eta) = \frac{2}{(2 + \eta)}\,(1 + \delta_M \eta^2/12) \tag{13}$$

namely, for Heyman-like distribution ($\delta_M = 0$), to

$$A^H(\eta) = \frac{2}{2 + \eta} \quad \text{or} \quad \eta^H(A) = 2\left(\frac{1}{A} - 1\right) \tag{14}$$

and, for Milankovitch-like distribution ($\delta_M = 1$), to

$$A^M(\eta) = \frac{12+\eta^2}{6(2+\eta)} \quad \text{or} \quad \eta^M(A) = 3A - \sqrt{3(3A^2+4A-4)} \tag{15}$$

while, from condition $h_e|_{\beta_r=0} = 0$, from Eq. (5) one gets, for η,

$$1 - \frac{\eta}{(2-\eta)}\,(1+\delta_M\eta^2/12) = 0 \tag{16}$$

leading to $\eta_l^H = 1$, and then $A_l^H = 2/3 = 0.\bar{6}$, for Heyman-like distribution, and to $\eta_l^M = 2(2\sqrt{3} - 3) \simeq 0.93$, and then $A_l^M = \sqrt{3} - 1 = 0.7320508075688773$, for Milankovitch-like distribution. The various characteristic values of the purely-rotational collapse states are later resumed in the forthcoming tables, reporting all together the main peculiar solution data, of the achieved analytical solution.

The regime of purely-overturning modes (at unbounded friction coefficient, $\mu \to \infty$), may actually continue until true physical Limit value $\eta_L = 2$ is reached ($t_L = 2r$), whereby $A_L^H = 1/2$ ($\alpha_L^H \simeq 159.7°$) and $A_L^M = 2/3$ ($\alpha_L^M \simeq 151.7°$) hold, setting the final limit for the rotational analysis, for Heyman-like and Milankovitch-like distributions, respectively. Trends $\eta(A)$ and $\eta(\alpha)$ for purely-overturning modes from Eqs. (14)-(15) are analytically drawn in Fig. 3, for the two distributions. Notice that $A(\alpha) = 2/3$ sets to zero the term under square root in Eq. (15), leading to $\eta = 2$, where a flat local vertical tangent is reached in either plot of Fig. 3 (with horizontal tangent in an inverse plot of either A or α as a function of η), on such $\eta = 2$ physical limit.

In practice, value $A(\alpha) = 2/3$ (α about 150°) constitutes a regional landmark, in terms of α, for collapse modes involving rotation, for both self-weight distributions. While Milankovitch-like solution ceases validity (for purely-overturning modes), Heyman-like solution ceases validity (for purely-rotational modes), then further extending, for purely-overturning modes, until $A(\alpha) = 1/2$ (which sets the limits, for $A(\alpha)$ and α, in the plots in Fig. 3). Thus, the validity range of rotational solutions, in terms of $A(\alpha)$ and α, turns out a bit narrower, for the real Milankovitch-like distribution. Despite, differences in the depicted narrow range of α, in the low plot reported in Fig. 3, keep quite limited, in terms of the η trends for purely-overturning modes from η_l up to $\eta_L = 2$.

Additionally, the purely-rotational solution, depicted in terms of η, as $\eta(\alpha)$ in the central plot of Fig. 2, and the purely-overturning solution, reported in Fig. 3, are analytically sketched, all together, in Fig. 4, in terms of both $\eta(A)$ and $\eta(\alpha)$, to appreciate the whole range of feasible solutions involving just joint rotation. In short, the trends from derived Eqs. (14)-(15) extend the range of the classical purely-rotational treatment [4, 8, 9], to handle as well purely-overturning modes, at further increasing α (decreasing $A(\alpha)$). Notice that trends sew together, C^1-continuously, at the shift from purely-rotational to purely-overturning modes, for both uniform self-weight distributions. Thereby, the physical value of Milankovitch-like distribution (slightly) limits the admissible range of real α states, with rapid, almost vertical growth of η toward $\eta = 2$. Roughly, the rotational least-thickness analysis is truly physically valid for half-opening angles up to about 150° (instead of about 160°, for the theoretical Heyman-like distribution).

Figures 3-4.

2.2 Sliding joint failure activation (at finite reducing friction)

The governing equations for sliding activation [3] are unmodified, from Heyman-like self-weight distribution, since weight resultants are unaffected, by Milankovitch-like distribution, just their positioning. Thus, they are confirmed as follows [6]:

- Sliding relation setting the activation of a shoulder sliding joint:

$$\mu = \mu_{ss}(\alpha, h) = \frac{h \sin\alpha - \alpha \cos\alpha}{h \cos\alpha + \alpha \sin\alpha} \qquad \text{or} \qquad h = h_{\mu}(\alpha, \mu) = \alpha \, \frac{\cos\alpha + \mu \sin\alpha}{\sin\alpha - \mu \cos\alpha} \tag{17}$$

- Sliding relation setting the activation of an inner sliding joint, which can be expressed by a stationary condition, at angular location $\beta = \beta_s$:

$$\mu = \mu_{is}(h) = \left. \frac{(1-h)\cos\beta - \beta \sin\beta}{(1-h)\sin\beta + \beta \cos\beta} \right|_{\beta \, = \, \beta_s(h) \, = \, \sqrt{h(1-h)}} \tag{18}$$

Recall that, as an important remark, at a joint sliding activation, finite friction coefficient μ sets the value of horizontal thrust h within the arch. Also, no dependence on thickness-to-radius ratio η is explicitly seen, in sliding Eqs. (17)-(18), similarly as for friction coefficient μ, in purely-rotational Eqs. (2)-(5), while sliding dependence on half-opening angle α is brought about just by shoulder sliding activation Eq. (17).

Purely-sliding collapse is set once both Eqs. (17)-(18) hold, which may be represented by solution triplet $\beta = \beta_s$, μ, h as a function of α [3]. Thus, once α or μ is set, μ or α is found, and h accordingly, with resulting inner sliding joint angular position at $\beta = \beta_s(h) = \sqrt{h(1-h)}$. The purely-sliding plot of $h(\alpha)$ is here included (black line), within that of the purely-rotational solution, in the bottom plot of Fig. 2. The function shall in principle be reported for α from 0 to π. However, as connected to the value of η, with non-apparent role in Eqs. (17)-(18), by rejoining them with rotational Eqs. (2)-(5), it will be seen that the practical α range for the purely-sliding mode will be confirmed to be limited from above, at Border point B with $\eta = 2$ ($t = 2r$), now at value $\alpha_B^M = 2.623074865083552 \simeq 150.3°$, with $\mu_B^M = 1.853774888450581$ ($\varphi_B^M \simeq 61.7°$). Thus, the (black) line in the bottom plot of Fig. 2 is set dashed (going flatly to 0 as $\alpha \to \pi$), after that α_B^M value, achieved for the Milankovitch-like distribution.

This importantly highlights and reconfirms the presence of **intersection Triple point T** among purely-rotational and purely-sliding $h(\alpha)$ lines, also for Milankovitch-like self-weight distribution, now occurring for the value of $\alpha_T^M = 2.430069103769349 \simeq 139.2°$, at non-dimensional horizontal thrust $h_T^M = 0.1147600824797408$, leading to $\beta_{s,T}^M = 0.3187321853045027 \simeq 18.3°$ and $\mu_T^M = 1.277021363435198$ ($\varphi_T^M \simeq 51.9°$), for the purely-sliding solution, and concomitantly to $\beta_{rT}^M = 1.042556808593598 \simeq 59.7°$ and $\eta^M = 0.6183182410743238$, for the purely-rotational Milankovitch solution. This again reveals and marks a joining link, and direct shift, between purely-rotational and purely-sliding solution.

Thus, this main discovery shows that this peculiar landmark separation is confirmed, for the Milankovitch-like self-weight distribution, which already hints that core qualitative features, on finite-friction effects, may not saliently be altered by the assumed distribution, and that conceptual separations and features of the solution may actually be similar, for both distributions. This is a principal crucial result of the present contribution, as demonstrated in what follows.

2.3 Mixed-mode failure activation

Resuming, for the whole present analytical treatment, toward the recognition of all self-standing domains and collapse states of the masonry arch, at variable inherent friction, including for **mixed rotational/sliding collapse**, for Milankovitch-like vs. Heyman-like uniform self-weight distribution:

- The first group of three underlying mechanical equations, Eqs. (2)-(5), affected by Milankovitch-like uniform self-weight distribution, through Milankovitch correction factor $fac_M = (1 + \delta_M \eta^2/12)$ and control flag δ_M ($\delta_M = 0$ for Heyman-like distribution; $\delta_M = 1$ for Milankovitch-like distribution), describes by itself the purely-rotational least-thickness solution, as classically stated by Heyman-like analysis, but with a correct imposition of the tangency of the line of thrust (locus of pressure points) at the masonry arch intrados [2, 4].

- The second group of two sliding relations, Eqs. (17)-(18), disregarding the role of the assumed uniform self-weight distribution, considers the possible activation of sliding joints, at the arch shoulder or/and at an inner sliding joint [6], and describes by itself the purely-sliding collapse mode.

Once part of the three purely-rotational equations and of the two sliding relations are active, mixed collapse mechanisms involving rotation/sliding may arise. The mechanical system is then ruled, in general, by 5 governing equations in terms of 5 variables, α, μ and η, h, $\beta = \beta_r$, while $\beta = \beta_s$ is implicitly represented as $\beta_s = \sqrt{h(1-h)}$.

3 Self-standing domains and collapse characteristics

The interplay of the above governing equations allows to derive a full map of the various manifestations of the considered mechanical system, in terms of admissible self-standing domains and collapse states, and separating boundaries between them. Primarily, as it was achieved for the H-like uniform self-weight distribution, a thickness-to-radius ratio vs. friction coefficient, η-μ two-dimensional projection diagram of the system (at implicitly variable half-opening angle α) can be derived, and depicted, with the representation of all admissible masonry arch states and collapse types, for the M-like uniform self-weight distribution, as compared to the H-like uniform self-weight distribution [3].

This is analytically drawn in the η-μ plots in Figs. 5-6, which constitute the true analytical map of the least-thickness solution, endowed with finite-friction effects, with main reported characteristic paths, landmark points and filled domains of collapse states, representing the salient condensing outcome of the present contribution. Thereby, intriguingly, all same conceptual and characteristic features earlier emerged for the H-like uniform self-weight distribution, as comprehensively described in [3], are newly confirmed, with similar results, for the M-like uniform self-weight distribution, even at increasing resulting η, appearing in Milankovitch correction factor $fac_M = (1 + \delta_M \eta^2/12)$.

Figures 5-6.

Specifically, the analytical maps of the dorsal lines dividing the domains of the various masonry arch states in the η-μ projection plane are first directly compared, for the M-like vs. H-like uniform self-weight distribution, in the two-dimensional η-μ plot reported in Fig. 5. Thereby, little detailed differences, in the outcomes for the two self-weight distributions may be appreciated, at increasing resulting η, especially in the higher η range among the asymptotic trends toward $\mu \to \infty$.

As recalled from [3], on behalf of the reader, the family of contemplated failure mechanisms of the symmetric circular masonry arch at variable inherent friction are confirmed to comprise the following seven collapse modes **[with indication of joints' type, among rotational (r) or sliding (s), raising from shoulder]**, correspondingly to the regions shaded in the further main filled η-μ analytical plot set in Fig. 6:

- purely-rotational (classical, correct, Heyman-like one) **[r,r,r]** (South-East);

- purely-sliding **[s,s]** (North-West);

- mixed sliding-rotational (with shoulder sliding) **[s,r,r]** (inner "pond" among the two above, up to characteristic Triple point T);

- mixed rotational-sliding (with inner sliding), with $\beta_r \geq \beta_s$ **[r,r,s]** (lower North-East "basin", still among the first two above, after Triple point T, upper bounded by shifting condition $\beta_r = \beta_s$, with manifested asymptotic trend for $\eta \to \eta_l$, $\eta_l^H = 1$ and $\eta_l^M = 2(2\sqrt{3} - 3) \simeq 0.93$, for H-like and M-like distributions, as $\mu \to \infty$);

- mixed rotational-sliding (with inner sliding), with $\beta_r \leq \beta_s$ **[r,s,r]** (same as above, now lower bounded by shifting condition $\beta_r = \beta_s$ and upper bounded by condition $\beta_r = 0$, with same manifested asymptotic trend);

- overturning-sliding ($\beta_r = 0$, with inner sliding and no block separation at the crown), for finite μ, at non-zero horizontal thrust h ruled by μ **[r,s]** (upper North-East "basin", lower bounded by condition $\beta_r = 0$ and upper bounded through physical limit $\eta \leq 2$);

- purely-overturning ($\beta_r = 0$, with two-block separation at the crown), for infinite μ and $\eta_l \leq \eta \leq 2$, at zero horizontal thrust h **[r]** (additional far-East boundary segment at $\mu \to \infty$ and $\eta_l \leq \eta \leq 2$).

The characteristics of the landmark points appearing along the main "continental divide" in the η-μ plots, wholly going from South-West to North-East, from $\eta = 0$ to $\eta = 2$, separating the arch states with collapse modes that do not (left) or do (right) display rotation (Fig. 6), are reported in Tables 1-2. Moreover, the earlier-derived data for the rotational asymptotic trends at $\mu \to \infty$, respectively limiting purely-rotational modes (becoming purely-overturning) and purely-overturning modes, are also gathered in Tables 3-4.

Tables 1-2 and 3-4.

Notice that, in the comparison among M-like and H-like distribution, the characteristic features recorded at the landmark points in the η-μ plots in Figs. 5-6, always show values that, for M-like vs. H-like distribution result (Tables 1-2):

- lower for thickness-to-radius ratio η (M-points below H-points);
- lower for friction coefficient μ (M-points left of H-points);
- lower for half-opening angle α (M-points reached earlier, than H-points, on ideal "iso-α" curves [3], at increasing α);
- higher non-dimensional horizontal thrust h, the arch being able to transfer in the least-thickness condition;
- wider angular position β_r for inner rotational joints;
- wider angular position β_s for inner sliding joints.

This shall mean that:

- Lower least-thickness and friction suffice for the arch to withstand, with higher transferred horizontal thrust, at those landmark states, for the M-like uniform self-weight distribution, though already reached at earlier half-opening angle, while increasing it. It reveals that the classical H-like uniform self-weight distribution (typically reasonable for contained values of η) anyway acquires conservative estimates, for the least-thickness self-standing condition, although the real α range results more limited.
- In practice, in the two-dimensional η-μ projection plot of the arch states in Fig. 5, M-like dorsals (and appointed peculiar landmark points; see points Triple T, Shift S, Junction J, Border B, in Fig. 6) result always below and left from H-like divides, while ideal M-like "iso-α" curves shall draw down below H-like ones (sketched in the η-μ plots presented in [3]).
- Accordingly, also the asymptotic trends for the purely-overturning solutions reached at unbounded friction, $\mu \to \infty$, along far right boundary segment $\eta_l \leq \eta \leq 2$ turn out lower, in terms of η, and α, for M-like vs. H-like distribution (see also detailed numerical data in Tables 3-4).

- Similarly, Border point B at physical limit value $\eta = 2$ ($t = 2r$) is reached for lower μ (much lower) and α, for M-like vs. H-like distribution, meaning again that, while a (much) lower μ suffices to reach a withstanding condition at $\eta = 2$, this is already achieved for a (slightly) narrower arch opening. Hereby, the higher difference, among M-like and H-like distribution, is appreciated, in seing a Border point B that collocates much on the left. This is likely the more apparent distinguished feature that is here discovered for the M-like self-weight distribution, in terms of detailed mechanical differences, by reading η-μ plots in Figs. 5-6, and associated results in Tables 1-2 and 3-4. In one sense, this was expected, in meaning that discrepancies could have been arising, at increasing η, from M-like correction factor fac_M, especially above the first asymptote for purely-rotational solutions (becoming purely-overturning), due to the expected increasing divergence from ideal H-like and true M-like distribution.

- Accordingly, this is for all the divide from Junction point J to Border point B, separating overturning-sliding states (right) and purely-sliding states (left), which deviates more, on the left, for M-like distribution, further at increasing η, arriving almost vertically at $\eta = 2$ (see also rotational plots in Figs. 3-4). This shows a sort of "saturation" effect, on friction coefficient μ, at increasing half-opening angle α (and thickness-to-radius ratio η), for the physical M-like distribution.

- Notice again that, as per the H-like distribution [3], a friction coefficient μ that is higher than that recorded at characteristic Triple point T, now at $\mu_T^M = 1.277021363435198$ ($\varphi_T^M \simeq 51.9°$), shall preclude any mixed sliding-rotational mode (with shoulder sliding and inner rotation), and at upper Border point B with $\eta = 2$, now at $\mu_B^M = 1.853774888450581$ ($\varphi_B^M \simeq 61.7°$), shall preclude any purely-sliding mode (with shoulder sliding and inner sliding).

- Correspondingly, mixed rotational-sliding modes (with shoulder rotation and inner sliding) are seen only on the right of Triple point T, and also peculiar mixed overturning-sliding modes (always with inner sliding) are recorded just on the right of Junction point J, here at $\mu_J^M = 1.546270800988723$ ($\varphi_J^M \simeq 57.1°$), meaning that, to prevent inner sliding activation, a higher friction coefficient is required, than for shoulder sliding activation, anyway setting the quest for increasing high-enough friction, to prevent sliding to appear within the masonry arch (see foreseen requirements to warrant third classical Heyman hypothesis of no sliding failure).

- In such a sense, the purely-overturning precarious equilibrium states that are reached among the two lower and upper asymptote values on η, η_l and $\eta_L = 2$, at variable α and zero horizontal thrust h (see limits in Tables 3-4), strictly require infinite friction to hold, to prevent concomitant inner sliding activation (at non-zero h).

- Dependencies on the angular positions of the inner rotational/slding joints, slightly wider (at less opened α), for M-like distribution, are flatter, for the two self-weight distributions, as these are being confirmed as a sort of internal ingredients, in the external appearance of masonry arch Mechanics, and resulting self-standings properties, in terms of main problem variables α, η, h, earlier enquired for purely-rotational modes, and, now, μ, in terms of induced finite-friction effects.

4 Illustration/validation by a numerical CP/MP formulation

As in source companion work [3], a separate confirmation and illustration of the achieved analytical outcomes is now provided, numerically, by running a dedicated, adapted, Complementarity Problem/Mathematical Programming (CP/MP) original formulation [7, 8], to validate and depict peculiar final results in terms of self-standing domains and collapse states of the (symmetric circular) masonry arch.

Hereby, the computational implementation has been updated, to handle the true M-like uniform self-weight distribution, with weight resultants' positioning as described in [4,8] (see Fig. 1), according to the effect of above-introduced Milankovitch correction factor $fac_M = (1 + \delta_M \, \eta^2/12)$ and associated on/off control flag δ_M, see Eqs. (2)-(5), which can be set on ($\delta_M = 1$), or off ($\delta_M = 0$), to account for the real M-like uniform self-weight distribution, or to the ideal, approximate, H-like uniform self-weight distribution, basically with the same arising computational burden.

As a main general concept, as typically outlined in the Theory of Plasticity, of Solids and Structures, masonry arch states can be governed by a Complementarity Problem, among strength conditions within static internal variables $\boldsymbol{\varphi}$ and collapse kinematic variables at rotating/sliding joints $\dot{\boldsymbol{\lambda}}$, which may further be brought down to a Mathematical Programming problem under linear constraints, with clear collapse onset that may numerically come out in the order of 10^{-16}, in the quest of a numerical zero for the sought minimum extremal condition, within a MatLab self-implementation of such an original "φ-λ formulation" (see computational details in [7, 8]):

$$\textbf{CP:} \quad \boldsymbol{\varphi} \leq \mathbf{0} \, , \quad \dot{\boldsymbol{\lambda}} \geq \mathbf{0} \, , \quad \boldsymbol{\varphi}^T \dot{\boldsymbol{\lambda}} = 0 \tag{19}$$

$$\Downarrow$$

$$\textbf{MP:} \quad \min \Big\{ - \boldsymbol{\varphi}^T \dot{\boldsymbol{\lambda}} \, | \, _{lin. \, constr.} \Big\} = 0 \tag{20}$$

As a consistent peculiar output, for the M-like uniform self-weight distribution, Figs. 7-12 report the typical masonry arches and collapse modes corresponding to the landmark points marked in the η-μ filled plot reported in Fig. 6, including for right segment boundary limits at $\mu \to \infty$, for $\eta = \eta_l^M$ and $\eta = 2$, and associated data reported in Tables 2 and 4, all together showing: geometrical features of the masonry arch in the least-thickness condition (black); strictly all-internal line of thrust (red) and line of friction (blue); symmetrically-set associated collapse mode, possibly including rotation/sliding (green).

Figures 7-12.

Specifically:

– Figs. 7-8 display the arch characteristics associated to Triple point T in the η-μ plane, with $\alpha_T^M = 2.430069103769349 \simeq 139.2°$ and $\mu_T^M = 1.277021363435198$ ($\varphi_T^M \simeq 51.9°$), and associated $\eta_T^M = 0.6183182410743238$, $h_T^M = 0.1147600824797408$ (see also intersection in bottom plot $h(\alpha)$

in Fig. 2), separating mixed sliding-rotational and mixed rotational-sliding modes, where also a direct shift from purely-rotational to purely-sliding modes is rejoined. Thereby, Fig. 7 shows the shift from purely-rotational (low) to purely-sliding (top) mode, while Fig. 8 illustrates the shift from mixed sliding-rotational (shoulder sliding, inner rotation; low) to mixed rotational-sliding (shoulder rotation, inner sliding; top) mode. Then, the four physical modes shown in Figs. 7-8 are concomitantly represented at Triple point T, while the associated mechanisms shall mathematically be obtained by any linear triple combination of three of them. Such a prominent watershed point displays, for the physical M-like uniform self-weight distribution, almost "rounded", easy to be remembered, and referred to, peculiar angular values, near to: $\alpha \simeq 140°$, $\varphi \simeq 52°$, $\beta_r \simeq 60°$, $\beta_s \simeq 20°$.

– Fig. 9 portrays the arch features corresponding to Shift point S where the main divide of the η-μ plot continuously reaches condition $\beta_r = \beta_s$, with $\alpha_S^M = 2.531269027051532 \simeq 145.0°$ and $\mu_S^M = 1.537913842804309$ ($\varphi_S^M \simeq 57.0°$), with shift from rotational-sliding mode (with $\beta_r = \beta_s$, whereby the same inner joint displays rotation and sliding, i.e. [r+s]; low) to purely-sliding mode (top). Also here, angular values turn out really "rounded", near to: $\alpha \simeq 145°$, $\varphi \simeq 57°$, $\beta_r = \beta_s \simeq 16°$.

– Fig. 10 depicts the arch characteristics corresponding to Junction point J where the η-μ dorsal reaches condition $\beta_r = 0$, with $\alpha_J^M = 2.534077907926732 \simeq 145.2°$ and $\mu_J^M = 1.546270800988723$ ($\varphi_J^M \simeq 57.1°$), with shift from mixed rotational(overtuning)-sliding mode (with $\beta_r = 0$; low) to purely-sliding mode (top). Being points S and J rather near, in the η-μ plot, associated peculiar values and angular positions are not really dissimilar (although notice that at Junction point J one has $\beta_r = 0$).

– Fig. 11 represents the arch properties corresponding to Border point B, on physical limit $\eta = 2$ ($t = 2r$), with $\alpha_B^M = 2.623074865083552 \simeq 150.3°$ and $\mu_B^M = 1.853774888450581$ ($\varphi_B^M \simeq 61.7°$), with shift from overturning-sliding (low) to purely-sliding (top) mode. Here, "rounded" angular values result about $\alpha \simeq 150°$, $\varphi \simeq 62°$, $\beta_s \simeq 14°$, with $\beta_r = 0$.

– Fig. 12 shows the two characteristic instances of purely-overturning mode with $h = 0$ at the extremes of the right boundary segment at $\mu \to \infty$ ($\varphi = 90°$), for $\eta_l \leq \eta \leq 2$, at $\eta = \eta_l^M = 2(2\sqrt{3} - 3) = 0.9282032302755092 \simeq 0.93$ ($\alpha_l^M = 2.590843443008955 \simeq 148.4°$, at $A_l^M = \sqrt{3} - 1$; low), and $\eta_L = 2$ ($\alpha_L^M = 2.648388899151005 \simeq 151.7°$, at $A_L^M = 2/3$; top). Here, then, about $\alpha \simeq 150°$, at $\varphi = 90°$ and $\beta_r = \beta_s = 0$.

This shall provide a comprehensive mechanical view of the salient characteristic features, for the considered least-thickness form-optimization problem of (symmetric circular) masonry arches (with radial joints), at reducing friction, for the true M-like uniform self-weight distribution, with qualitative characteristics that appear rather similar to those earlier experienced in [3], for the classical H-like uniform self-weight distribution, and with little quantitative discrepancies at raising resulting η, say roughly in the region above and right Triple point T in the η-μ plot, and especially in the basin of overturning-sliding modes from Junction point J to Border point B, with η ranging from about 0.9 to 2.

5 Conclusions

The present contribution has analytically investigated the role of inherent finite friction, in the classical least-thickness form optimization problem of self-standing (symmetric circular) masonry arches ("Couplet-Heyman problem"), as a sort of addendum to previous work [3], whereby a classical Heyman-like uniform self-weight distribution along geometrical centreline of the arch was considered, while here results are newly derived, for the true Milankovitch-like uniform self-weight distribution accounting for the real centres of gravity of the ideal wedge-shaped chunks of the arch, endowed with radial stereotomy, and compared, with possible expected discrepancies at increasing resulting least thickness of the masonry arch.

Despite, all salient conceptual features and characteristics, of self-standing states and collapse modes of the masonry arch, have intriguingly been confirmed, with some little deviations, in the technical details and related outcomes, becoming more evident just in the thick-arch range around and above the limit value of least thickness recorded for purely-rotational modes at infinite friction.

Importantly, the class of all types of collapse modes is enumerated and confirmed, with respect to the previous analysis, with updated physical results, in terms of required friction (as linked to classical third Heyman hypothesis of no sliding failure), which may shortly be summarized as follows, having in mind the main two-dimensional traced maps of thickness-to-radius ratio η vs. friction coefficient μ (friction angle φ) in Figs. 5-6, at implicitly variable half-opening angle α of the symmetric circular masonry arch, of the mechanical system states:

- a friction coefficient of about $\mu \simeq 1.277$ ($\varphi \simeq 52°$, say around 50°; look at Triple point T) shall suffice to prevent any mixed sliding-rotational mode of the arch (with shoulder sliding and inner rotation).
- on the left of that (Triple point T), mixed sliding-rotational modes may subsist even at further reducing friction, at lowering arch opening (α lower than about $2.43 \simeq 139°$, say around 140°), and least-thickness. Most common cases of undercomplete arches or slightly overcomplete arches, shall lie into this range. For instance, for the typical case of the complete, semicircular arch, a characteristic value of about $\mu \simeq 0.395$ ($\varphi \simeq 22°$, say around 20°) shall suffice to prevent shoulder sliding activation, and warrant Heyman-like purely-rotational collapse in the least-thickness condition.
- on the right of that (Triple point T), mixed rotational-sliding modes (with shoulder rotation and inner sliding) may appear, with a necessary parallel increase of η and μ.
- at increasing opening angle, the friction coefficient necessary to prevent sliding modes raises, and requires an unbounded value in the limit case of purely-rotational modes and purely-overturning modes.
- the latter, rather precarious self-standing states (theoretically holding just at infinite friction), come to lie in the thick-arch range and, within that, finite friction anyway leads to further inner-joint sliding, in shifting from purely-overturning to overturning-sliding modes.
- a friction coefficient of about $\mu \simeq 1.854$ ($\varphi \simeq 62°$, say around 60°; look at Border point B at limit physical value $\eta = 2$) shall suffice to prevent any purely-sliding mode to appear for the arch.

Further general and specific itemized resuming considerations, about context and value of the present paper, relevance and framing of the current finite-friction analysis, and confrontation of outcomes from assumed Milankovitch-like vs. Heyman-like uniform self-weight distribution, added at review stage, may briefly be outlined as follows:

- The paper has considered the so-called "Couplet-Heyman problem", of least-thickness optimization, as a fundamental setting, in the general understanding of the Mechanics (Statics) of masonry arches and structures. Focus is placed on the issue of finite friction, disregarded by classical Heyman treatment. The solution is first derived by a full original analytical approach, and illustrated by "exact" analytical plots and digital results. Then, it has separately been validated, and further illustrated, by an original numerical implementation of a Complementarity Problem/Mathematical Programming (CP/MP) "φ-λ formulation" by the Authors. The achieved results compare the outcomes, of the two assumed uniform self-weight distributions, by Heyman and Milankovitch, with reference to the issue of finite friction, and its implications in the arising collapse modes.

- The paper reports full original research work, with achieved unprecedented results, which are condensed in full analytical plots, outlined in Figs. 2-6. Numerical illustration results on arch forms in Figs. 7-12 are as well innovative, and shall provide a clear panorama, on the various arch settings, and resulting collapse mechanisms. Herein, main literature reference [1–10] was restricted to the information strictly needed for the analytical derivation, on behalf of the reader, and to provide the means to allow, in principle, to independently reproduce the new analytical solution, as required in standard scientific publishing. A further, comprehensive literature framing was assembled in source paper [3], referring to various approaches of analysis, in the handling of similar problems for masonry arches and structures.

- The achieved analytical-numerical outcomes look wholly consistent, and considerably extend, earlier prodromic results provided in the pertinent scientific literature on masonry arches and structures, as specifically linked to the investigation of finite-friction effects, in the structural capacity of masonry structures [11–26], which have provided a rather solid basis and reference methodological framework, with specific devoted tools of analysis, by different graphical-analytical and numerical strategies, to be complemented, still, by additional, systematic rational treatments, specifically once analytically pursued, whenever possible, as herein primarily sought (within the framework of symmetric circular masonry arches). In particular, within that, the achieved main analytical η-μ representations (Figs. 5-6) appear coherent with similar finite-friction results earlier reported e.g. in [13, 14, 18, 24], and generalize them the a full spectrum of arch morphological features and inherent properties.

- Specifically, and importantly, in the present setting, of symmetric circular masonry arches, under uniform self-weight, as per the earlier derived results for the Heyman-like uniform self-weight distribution in [3], no issues of potential non-uniqueness, here in terms of least-thickness evaluation, at given arch characteristics, as linked to the non-normality of the flow rule, have been recorded, even for the Milankovitch-like uniform self-weight distribution, by both the analytical solution and the numerical solution. Notice that the latter,

numerical CP/MP formulation, specifically, shall indeed account for the possible manifestation of such effects, and was actually conceived to investigate that, being able, in principle, to correctly link both static and kinematic descriptions, in the incipient collapse condition, and then to provide all consistent solutions. Indeed, in general, as stated by Drucker [11], whereby *"It is shown that the limit theorems previously proved for assemblages of perfectly plastic bodies do not always apply when there is finite sliding friction"*, non-uniqueness in load multiplier (herein thickness-to-radius ratio) evaluation may possibly occur. Despite, uniqueness may still hold in some class of problems [17–19], as Gilbert et al. [18] were affirming that *"Casapulla and Lauro (2000) have identified a special class of non-associative friction problems for which provably unique solutions exist. The class comprises arches with symmetrical loading and geometry."*, as it is indeed recovered in the present case. These outcomes have also later been confirmed and discussed in [24–26]. Despite, further, general analytical and numerical formulations shall investigate the subject, in inspecting if friction reduction effects may induce a resulting non-uniqueness in the prediction of the least-thickness condition, as instead still recorded in the present setting devoted to the analysis of symmetric masonry arches under uniform self-weight, for more unspecific configurations and loading conditions.

- The original, self-made CP/MP numerical implementation, by the Authors (Section 4), is indeed conceived and taken, herein, for numerical validation and illustration purposes, given the fact that other standard, possibly available, numerical tools, as general or specific FEM or DEM codes, would be quite inappropriate or un-useful, to provide a direct quantitative comparison to the fineness of the derived "exact" analytical results (look for instance at the digital outcomes, in provided Tables 1-4). Moreover, comparison to a DEM-like (DDA) formulation, made publically available by others, was already attempted, by the Authors, in some of the mentioned previous works (see [5, 8]). To avoid repetition, but mainly to go much beyond that, an original self-made implementation was indeed ad hoc scheduled, and systematically adopted, herein in the context of the Milankovitch-like uniform self-weight distribution, to quantitatively reveal the effects of inherent friction, in the present setting.

- Indeed, the main value of the paper shall lay in contributing to the basic understanding of the Mechanics of masonry arches and structures. Also, it is felt, within that, that the value of "exact" analytical solutions, as pursed, and fully achieved in the paper, shall provide a universal way of comprehension and of independent reproduction, of fundamental problems, setting a way, of rational reasoning, also once dealing with practical contexts, in real-world architectural and engineering applications, in terms of final implications, when collapse modes should be studied, to be prevented to occur.

- About value of Milankovitch-like vs. Heyman-like uniform self-weight distribution, and relevant mechanical description, and outcomes, it would not generally be claimed of "advantages", among adopting one or the other. The Milankovitch-like distribution is simply the true one, the Heyman-like being instead an approximate one, increasingly as thickness grows. Despite, it adds some little complexity, in the analytical settings, as challenged, successfully, in the paper. In the numerical implementation, instead, it can easily be flagged (Section 4), to be shifted upon, to get finest results, at basically the same compu-

tational cost. In one sense, it should always be made reference to the Milankovitch-like distribution, though the positioning to the classical, Heyman-like distribution, is always fundamental, given its wide use, and actual validity, for arch openings that do not go beyond complete semicircular arches, where, since the resulting critical thickness keeps small, the recorded differences turn out quite marginal, while the theoretical treatment stays simpler. Instead, for horseshoe arches, differences somehow increase, in numerical terms, though, interestingly, conceptual results remain the same, and this is one main achievement of the paper, since this may perhaps be conjectured, but was rather unsure, before undertaking the analysis. For this reason, it is felt this to be a crucial, innovative contribution, to the dedicated literature on masonry constructions.

- The various arch illustrations depicted in Figs. 7-12, as introduced in text in Section 4, right after Eq. (20), refer to the main points on the paths in the fundamental thickness-to-radius ratio/friction coefficient plane (see Figs. 5-6). The arch illustrations may be confronted to similar illustrations, adopted in source paper [3], for the Heyman-like distribution. Though qualitative outcomes look similar, for the two self-weight distributions, quantitative results turn out somehow different, as also reported in the tables, and in the shown figures, and their captions, which anyhow refer to wide-opened arches, where differences raise more, and can much be appreciated.

In conclusion, the achieved outcomes shall then provide a consolidated picture and a main guideline in the analysis of finite-friction effects for such an iconic optimization problem in the Mechanics of (symmetric circular) masonry arches, toward general understanding of basic features and warranting fundamental structural bearing capacity.

Further specific aspects may additionally be deepened, within the present mechanical analysis, for diverse subtle issues and points that may likewise be inspected, as e.g. that of the above-mentioned potential non-uniqueness issue, of extremal load bearing capacity, at finite friction, to achieve even a wider complete and detailed understanding, of the various underlying multi-faceted features, in the present framework, and in generalized ones, where different arch forms or characteristics may moreover be considered, both analytically, as here pursued, whenever possible, or numerically, for instance through the stated Complementarity Problem/Mathematical Programming original "φ-λ formulation", and possibly adapted selected computational implementations, even in the realm of the numerical analysis of physical arch structural morphologies and external conditions.

Acknowledgments

This work has been developed at the University of Bergamo, School of Engineering (Dalmine). The support by ministerial (MUR) funding "Fondi di Ricerca d'Ateneo ex 60%" at the University of Bergamo is gratefully acknowledged.

Compliance with Ethical Standards

The authors declare that they have no conflict of interest.

References

[1] Milankovitch, M. (1907). Theorie der Druckkurven, Zeitschrift für Mathematik und Physik, 55, pp. 1-27.

[2] Heyman, J. (1969). The safety of masonry arches, International Journal of Mechanical Sciences, 11(4), pp. 363-385. DOI: 10.1016/0020-7403(69)90070-8.

[3] Cocchetti, G., Rizzi, E. (2024). Finite-friction least-thickness self-standing domains of symmetric circular masonry arches, Structures, Special Issue on Shells and Spatial Structures: Conceptual Design, Construction and Maintenance, Accepted 19 June 2024, Published online 8 July 2024, 66(August 2024), Paper 106800, pp. 1-20, available Open Access at https://www.sciencedirect.com/science/article/pii/S2352012424009524. DOI: 10.1016/j.istruc.2024.106800.

[4] Cocchetti, G., Colasante, G., Rizzi, E. (2011). On the analysis of minimum thickness in circular masonry arches. Part I: State of the art and Heyman's solution. Part II: Present CCR solution. Part III: Milankovitch-type solution, Applied Mechanics Reviews, ASME, September 01, 2011, 64(5), Paper 050802 (Oct. 01, 2012), pp. 1-27. DOI: 10.1115/1.4007417.

[5] Rizzi, E., Rusconi, F., Cocchetti, G. (2014). Analytical and numerical DDA analysis on the collapse mode of circular masonry arches, Engineering Structures, 60(February 2014), pp. 241-257. DOI: 10.1016/j.engstruct.2013.12.023.

[6] Cocchetti, G., Rizzi, E. (2020). Analytical and numerical analysis on the collapse modes of least-thickness circular masonry arches at decreasing friction, Frattura ed Integrità Strutturale - Fracture and Structural Integrity, Special Issue on: Fracture and Damage Detection in Masonry Structures, 14(51), pp. 356-375, available Open Access at https://www.fracturae.com/index.php/fis/article/view/2554. DOI: 10.3221/IGF-ESIS.51.26.

[7] Cocchetti, G., Rizzi, E. (2020). Non-linear programming numerical formulation to acquire limit self-standing conditions of circular masonry arches accounting for limited friction, International Journal of Masonry Research and Innovation, Special Issue on: 10IMC Masonry Research in the Third Millennium From Theory to Practical Applications, 5(4), pp. 569-617. DOI: 10.1504/IJMRI.2020.111806.

[8] Cocchetti, G., Rizzi, E. (2020). Static upper/lower thrust and kinematic work balance stationarity for least-thickness circular masonry arch optimization, Journal of Optimization Theory and Applications, Special Issue on: Computational Optimization for Structural Engineering and Applications, 187(3), pp. 707-757, available Open Access at https://link.springer.com/article/10.1007/s10957-020-01772-0. DOI: 10.1007/s10957-020-01772-0.

[9] Cocchetti, G., Rizzi, E. (2021). Least-thickness symmetric circular masonry arch of maximum horizontal thrust, Archive of Applied Mechanics, 91(6), pp. 2617-2639, available Open Access at https://link.springer.com/article/10.1007/s00419-021-01909-1. DOI: 10.1007/s00419-021-01909-1.

[10] Blasi, C., Foraboschi, P. (1994). Analytical approach to collapse mechanisms of circular masonry arch, Journal of Structural Engineering, ASCE, 120(8), pp. 2288-2309. DOI: 10.1061/(ASCE)0733-9445(1994)120:8(2288).

[11] Drucker, D.C. (1954). Coulomb friction, plasticity, and limit loads, Journal of Applied Mechanics, 21(1), pp. 71-74. DOI: 10.1115/1.4010821.

[12] Boothby, T.E. (1994). Stability of masonry piers and arches including sliding, Journal of Engineering Mechanics, ASCE, 120(2), pp. 304-319. DOI: 10.1061/(ASCE)0733-9399(1994)120:2(304).

[13] Sinopoli, A., Corradi, M., Foce, F. (1997). Modern formulation for preelastic theories on masonry arches, Journal of Engineering Mechanics, ASCE, 123(3), pp. 204-213. DOI: 10.1061/(ASCE)0733-9399(1997)123:3(204).

[14] Sinopoli, A., Aita, D., Foce, F. (2007). Further remarks on the collapse mode of masonry arches with Coulomb friction, Proc. of 5th Int. Conference on Arch Bridges (ARCH'07), Funchal, Madeira, Portugal, September 12-14, 2007, P.B. Lourenço, D.B. Oliveira, A. Portela (Eds.), Multicomp, Lda Publishers, Madeira, pp. 649-657.

[15] Baggio, C., Trovalusci, P. (2000). Collapse behaviour of three-dimensional brick-block systems using non-linear programming, Structural Engineering and Mechanics, 10(2), pp. 181-195. DOI: 10.12989/sem.2000.10.2.181.

[16] Rios, A.J., Nela, B., Pingaro, M., Reccia, E., Trovalusci, P. (2025). Parametric analysis of masonry arches following a limit analysis approach: Influence of joint friction, pier texture, and arch shallowness, Mathematics and Mechanics of Solids, OnlineFirst 11 July 2023, 30(1), pp. 137-165. DOI: 10.1177/10812865231175385.

[17] Casapulla, C., Lauro, F. (2000). A simple computation tool for the limit-state analysis of masonry arches, Proc. of 5th Int. Congress on Restoration of Architectural Heritage, Università di Firenze, 17-24 September 2000, CDROM Proc., pp. 2056-2064, 9 pages.

[18] Gilbert, M., Casapulla, C., Ahmed, H.M. (2006). Limit analysis of masonry block structures with non-associative frictional joints using linear programming, Computers and Structures, 84(13-14), pp. 873-887. DOI: 10.1016/j.compstruc.2006.02.005.

[19] D'Ayala, D., Tomasoni, E. (2011). Three-dimensional analysis of masonry vaults using limit state analysis with finite friction, International Journal of Architectural Heritage, 5(2), pp. 140-171. DOI: 10.1080/15583050903367595.

[20] Trentadue, F., Quaranta, G. (2013). Limit analysis of frictional block assemblies by means of fictitious associative-type contact interface laws, International Journal of Mechanical Sciences, 70 (May 2013), pp. 140-145. DOI: 10.1016/j.ijmecsci.2013.02.012.

[21] Trentadue, F., De Tommasi, D., Marasciuolo, N., Vitucci, G. (2024). Thrust in a symmetric masonry arch with frictional joints on spreading supports, Acta Mechanica, 235(2), pp. 659-670. DOI: 10.1007/s00707-023-03759-0.

[22] Bagi, K. (2014). When Heyman's Safe Theorem of rigid block systems fails: Non-Heymanian collapse modes of masonry structures, International Journal of Solids and Structures, 51(14), pp. 2696-2705. DOI: 10.1016/j.ijsolstr.2014.03.041

[23] Gáspár, O., Sajtos, I., Sipos, A.A. (2021). Friction as a geometric constraint on stereotomy in the minimum thickness analysis of circular and elliptical masonry arches, International Journal of Solids and Structures, 225(15 August 2021), 111056, pp. 1-18. DOI: 10.1016/j.ijsolstr.2021.111056.

[24] Aita, D., Barsotti, R., Bennati, S. (2019). Looking at the collapse modes of circular and pointed masonry arches through the lens of Durand-Claye's stability area method, Archive of Applied Mechanics, 89(8), pp. 1537-1554. DOI: 10.1007/s00419-019-01526-z.

[25] Aita, D., Sinopoli, A. (2021). Two different approaches for collapse of nonsymmetric masonry arches: Monasterio's treatment versus limit equilibrium analysis, Journal of Engineering Mechanics (ASCE), 147(10), 04021071, pp. 1-18. DOI: 10.1061/(ASCE)EM.1943-7889.0001989.

[26] Aita, D., Beatini, V, Caruso, H., Garavaglia, E., Sgambi, L. (2025). Some remarks on non-standard plastic behaviour with Coulomb's friction starting from an unconventional stone flat arch, Engineering Structures, 326(1 March 2025), 119539, pp. 1-15. DOI: 10.1016/j.engstruct.2024.119539.

Tables and Figures

H	(T) Triple point	(S) Shift point	(J) Junction point	(B) Border point
η	0.6796047320988860	0.9533663968209255	0.9652414772084208	2
μ	1.415270827756886	1.765868462744654	1.777213608388237	2.690297881776622
α	2.487161163767182	2.600211150484514	2.603266515104794	2.774176793356034
h	0.09780581933963814	0.06791978142522512	0.06718190191428895	0.03200476409857036
β_r	1.037485213550072	0.2516081968386061	0	0
β_s	0.2970519164101457	0.2516081968386061	0.2503367611228279	0.1760126676508405

Table 1: Characteristic data of peculiar landmark points along the divide in the η-μ plane: Heyman-like uniform self-weight distribution.

M	(T) Triple point	(S) Shift point	(J) Junction point	(B) Border point
η	0.6183182410743238	0.8734660698200912	0.8872221963291936	2
μ	1.277021363435198	1.537913842804309	1.546270800988723	1.853774888450581
α	2.430069103769349	2.531269027051532	2.534077907926732	2.623074865083552
h	0.1147600824797408	0.08555323265580009	0.08479836323759742	0.06248908922171234
β_r	1.042556808593598	0.2797031945436853	0	0
β_s	0.3187321853045027	0.2797031945436853	0.2785814079040845	0.2420417380328302

Table 2: Characteristic data of peculiar landmark points along the divide in the η-μ plane: Milankovitch-like uniform self-weight distribution.

	Heyman-like distribution limits	
	low asymptote	top asymptote
η	1	2
$A(\alpha) = \alpha \cot(\alpha/2)$	$2/3 = 0.\bar{6}$	$1/2 = 0.5$
α	$2.648388899151005 \simeq 151.7°$	$2.786498150651177 \simeq 159.7°$

Table 3: Characteristic data of limit points for purely-overturning modes at $\mu \to \infty$ ($\varphi = 90°$): Heyman-like uniform self-weight distribution.

	Milankovitch-like distribution limits	
	low asymptote	top asymptote
η	$2(2\sqrt{3} - 3) = 0.9282032302755092$	2
$A(\alpha) = \alpha \cot(\alpha/2)$	$\sqrt{3} - 1 = 0.7320508075688773$	$2/3 = 0.\bar{6}$
α	$2.590843443008955 \simeq 148.4°$	$2.648388899151005 \simeq 151.7°$

Table 4: Characteristic data of limit points for purely-overturning modes at $\mu \to \infty$ ($\varphi = 90°$): Milankovitch-like uniform self-weight distribution.

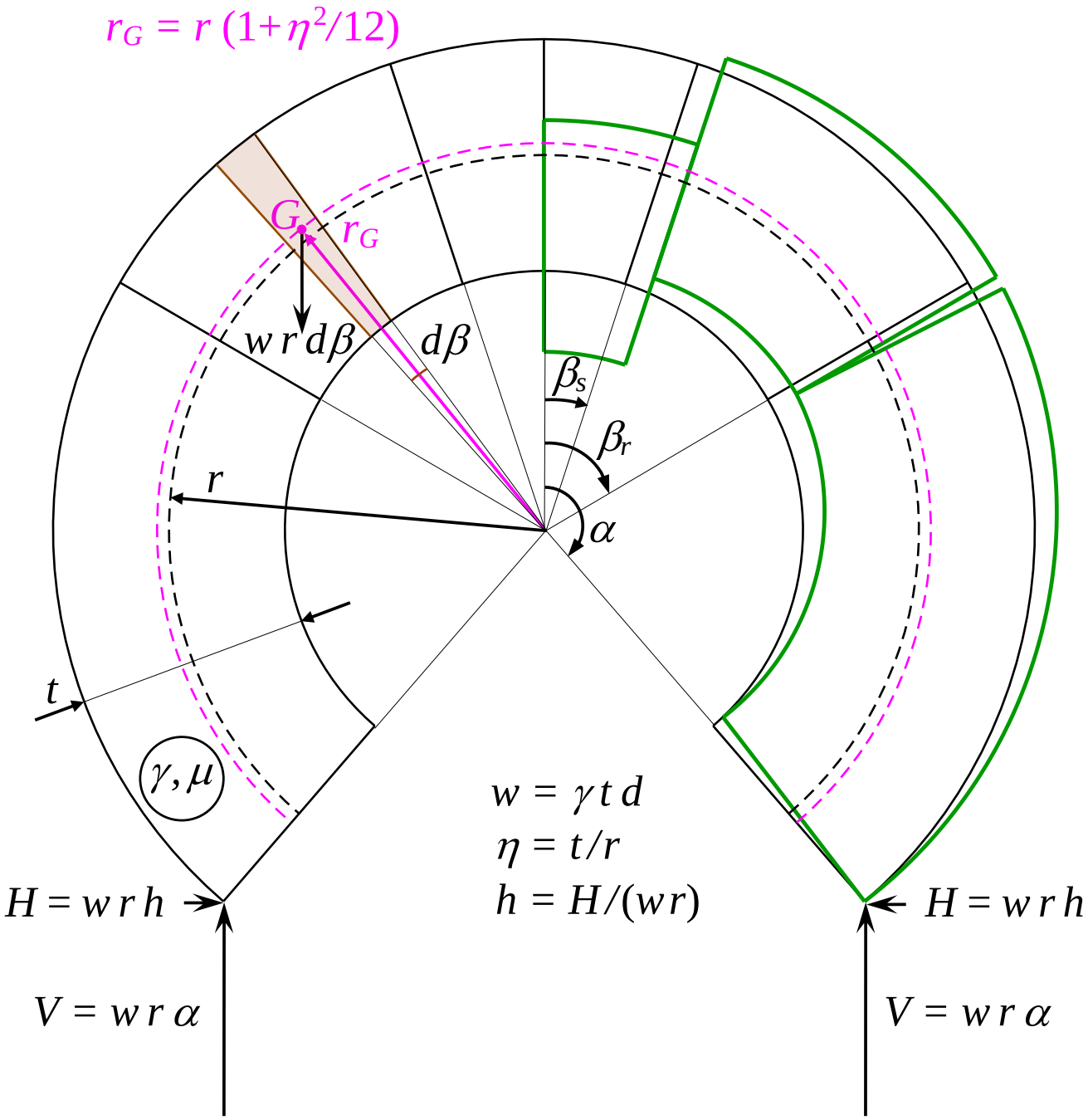

Figure 1: Analytical sketch of a self-standing symmetric circular continuous masonry arch with inner radius r, thickness t (thickness-to-radius ratio $\eta = t/r$), out-of-plane depth d, uniform specific weights per unit volume γ and per unit length of geometrical centreline of the arch $w = \gamma t d$, and inherent friction coefficient μ, with indication of the various characteristic variables (horizontal shoulder reaction H opposite of horizontal thrust H, and non-dimensional horizontal thrust $h = H/(wr)$, vertical shoulder reaction V opposite of half-arch weight $W = wr\alpha$; half-angle of embrace α, sliding β_s and rotational β_r angular inner-joint positions from the crown). The plot specifically refers to the arch features for the overcomplete case of landmark "Triple point T", displaying concomitant multiple (four) underlying collapse modes: purely-rotational, purely-sliding, mixed rotational-sliding, mixed sliding-rotational. The mixed rotational-sliding mechanism (of the half-arch) is selectively represented on the right. On the left, an infinitesimal arch element with real centroid G, for true Milankovitch-like uniform self-weight distribution at radial distance $r_G = r(1 + \eta^2/12)$, versus classical approximate Heyman-like uniform self-weight distribution at radial distance r, is depicted.

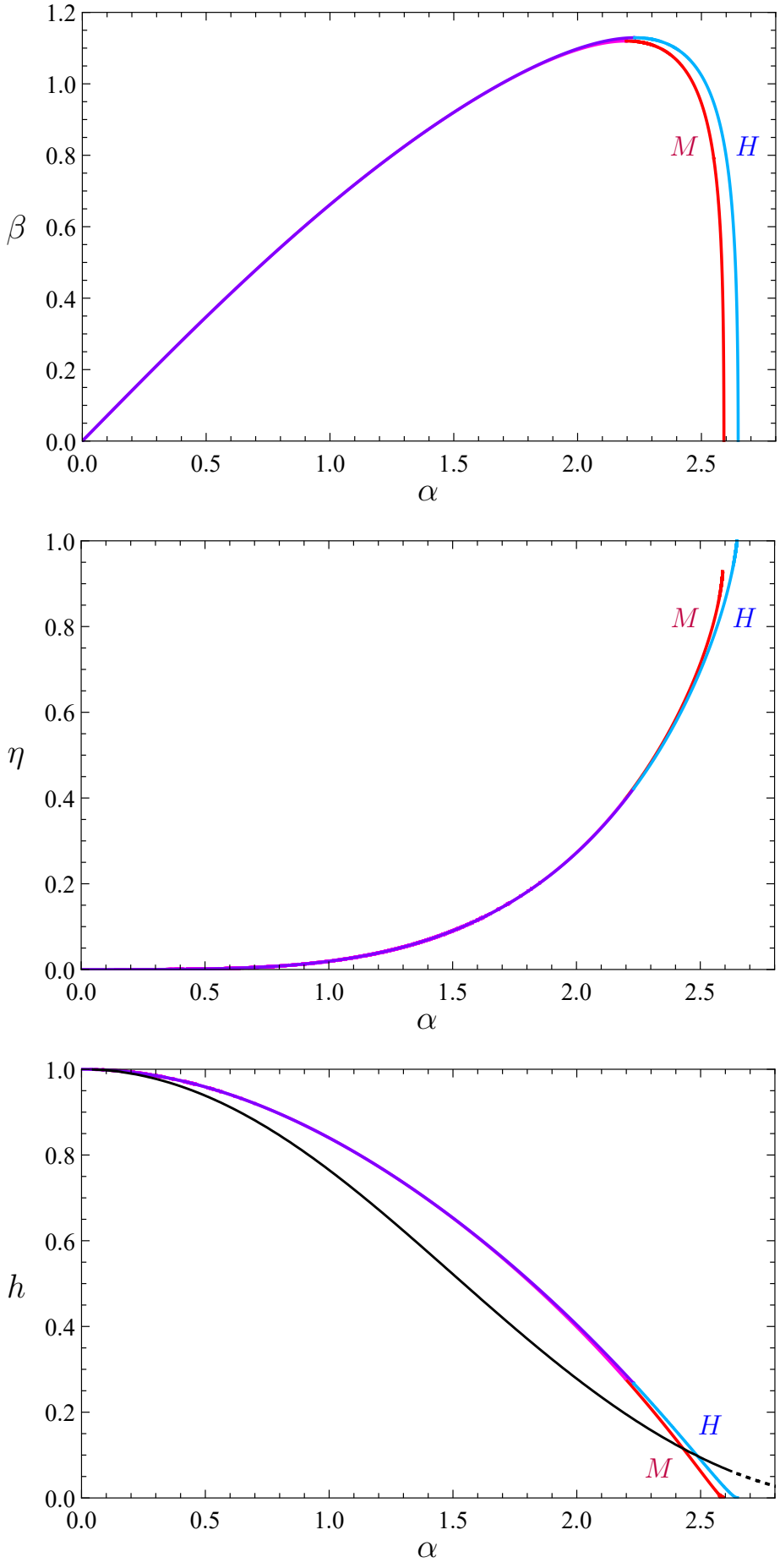

Figure 2: Purely-rotational least-thickness M/H-like solutions (purple/blue) for solution triplet $\beta = \beta_r, \eta, h$ as a function of α, with bottom purely-sliding $h(\alpha)$ trend (black).

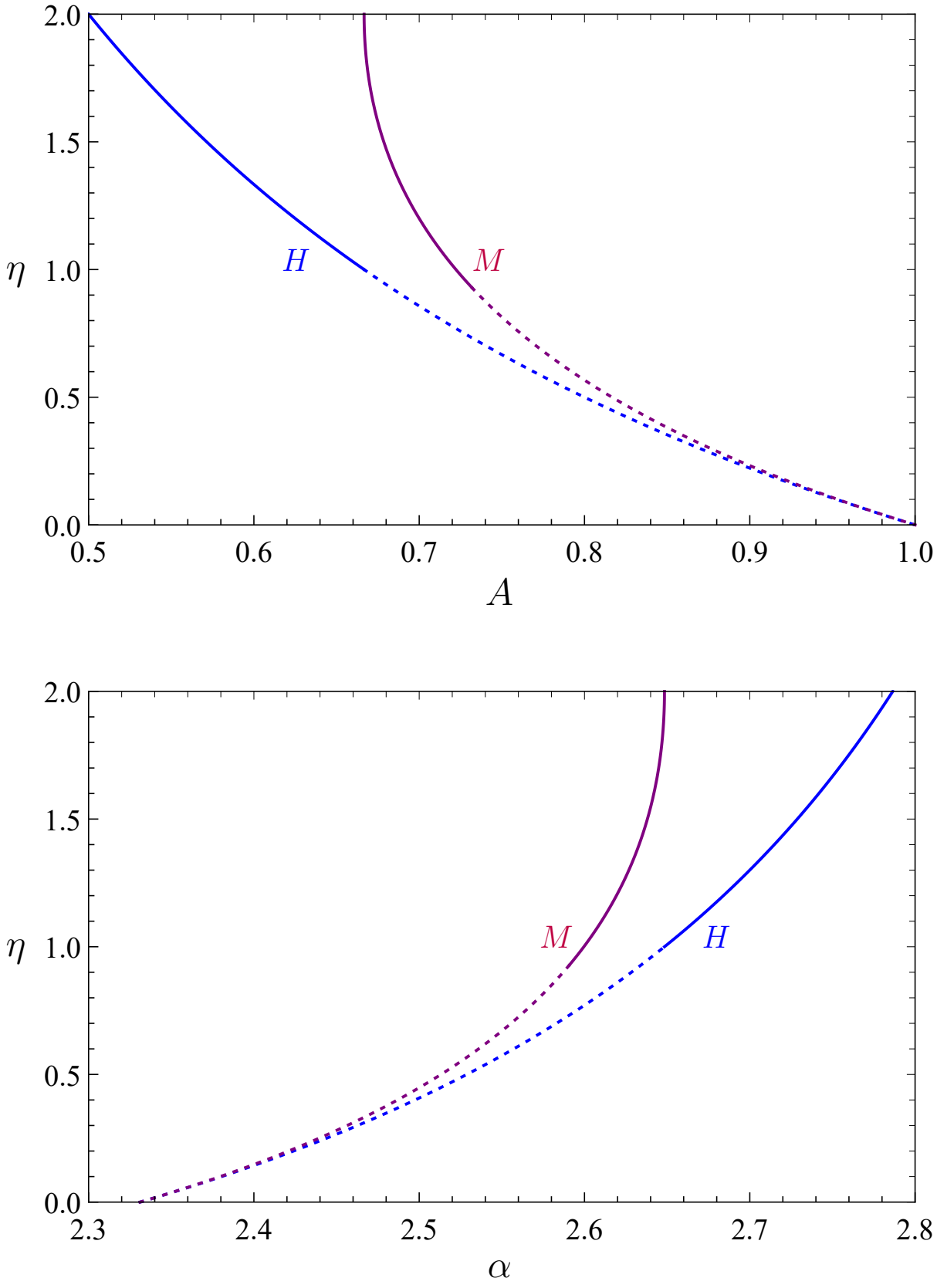

Figure 3: Purely-overturning M/H-like trends η of A and η of α.

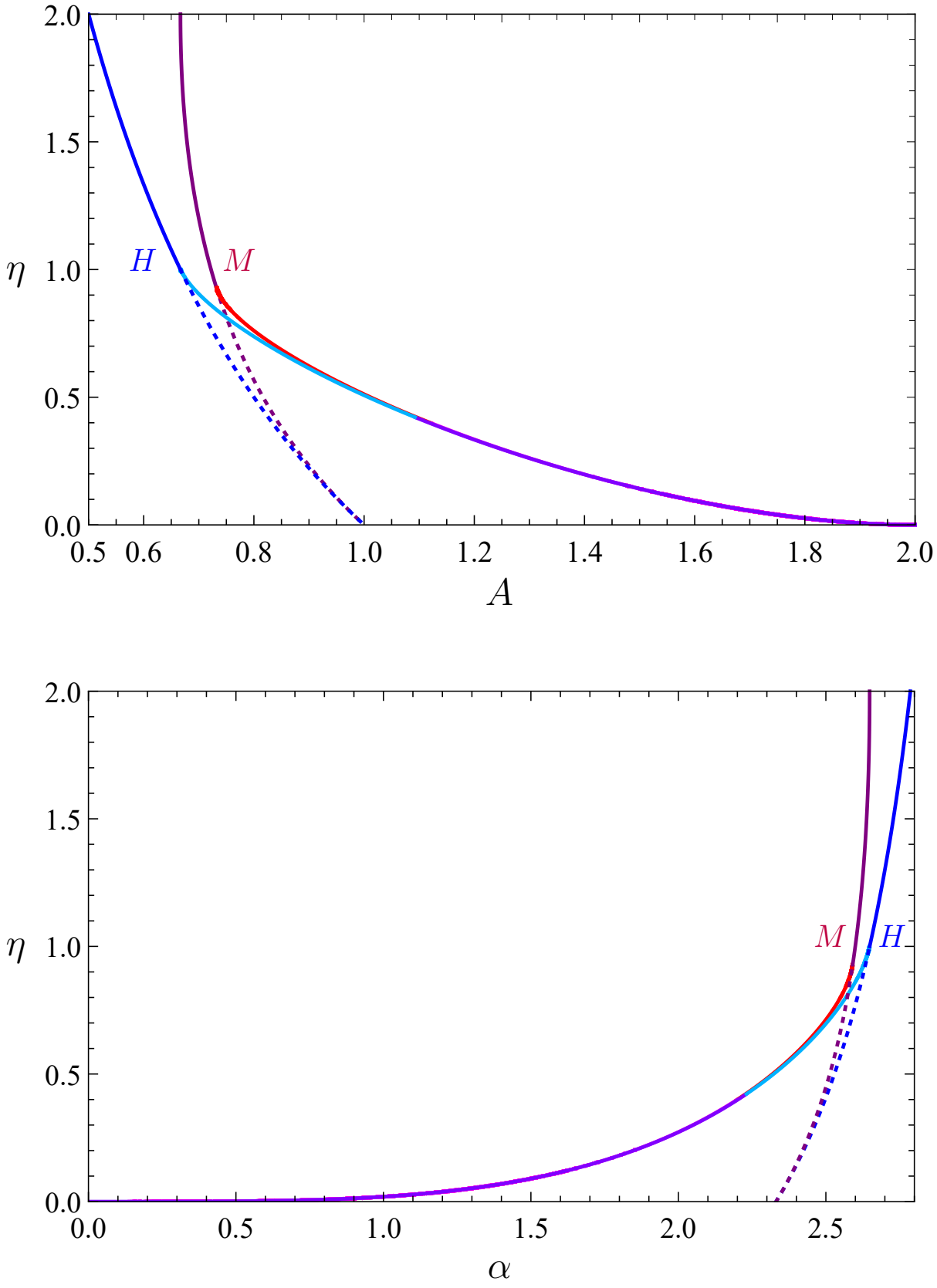

Figure 4: Purely-rotational/purely-overturning M/H-like trends η of A and η of α.

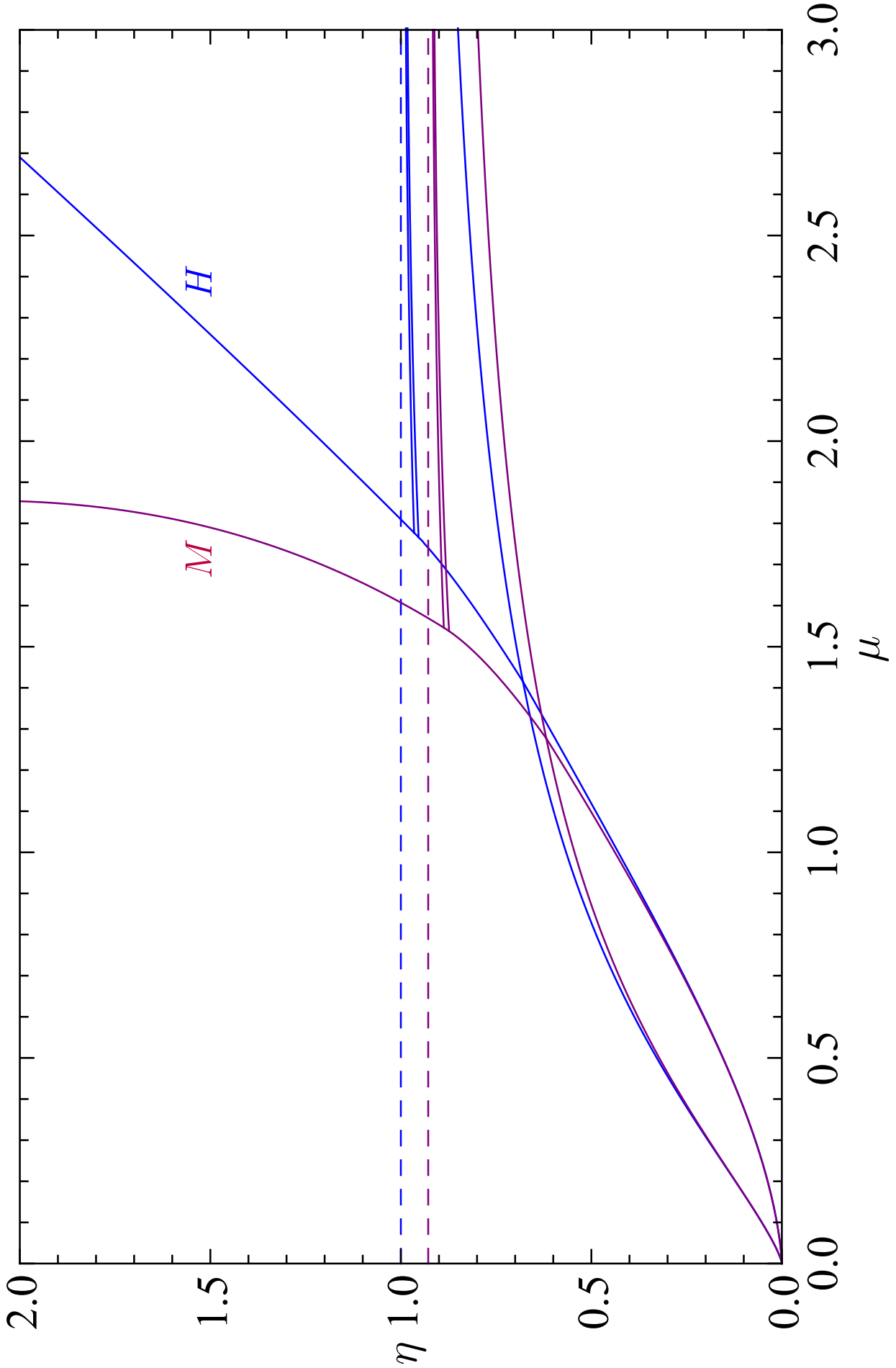

Figure 5: Analytical η-μ maps of self-standing and collapse states for M/H-like distributions.

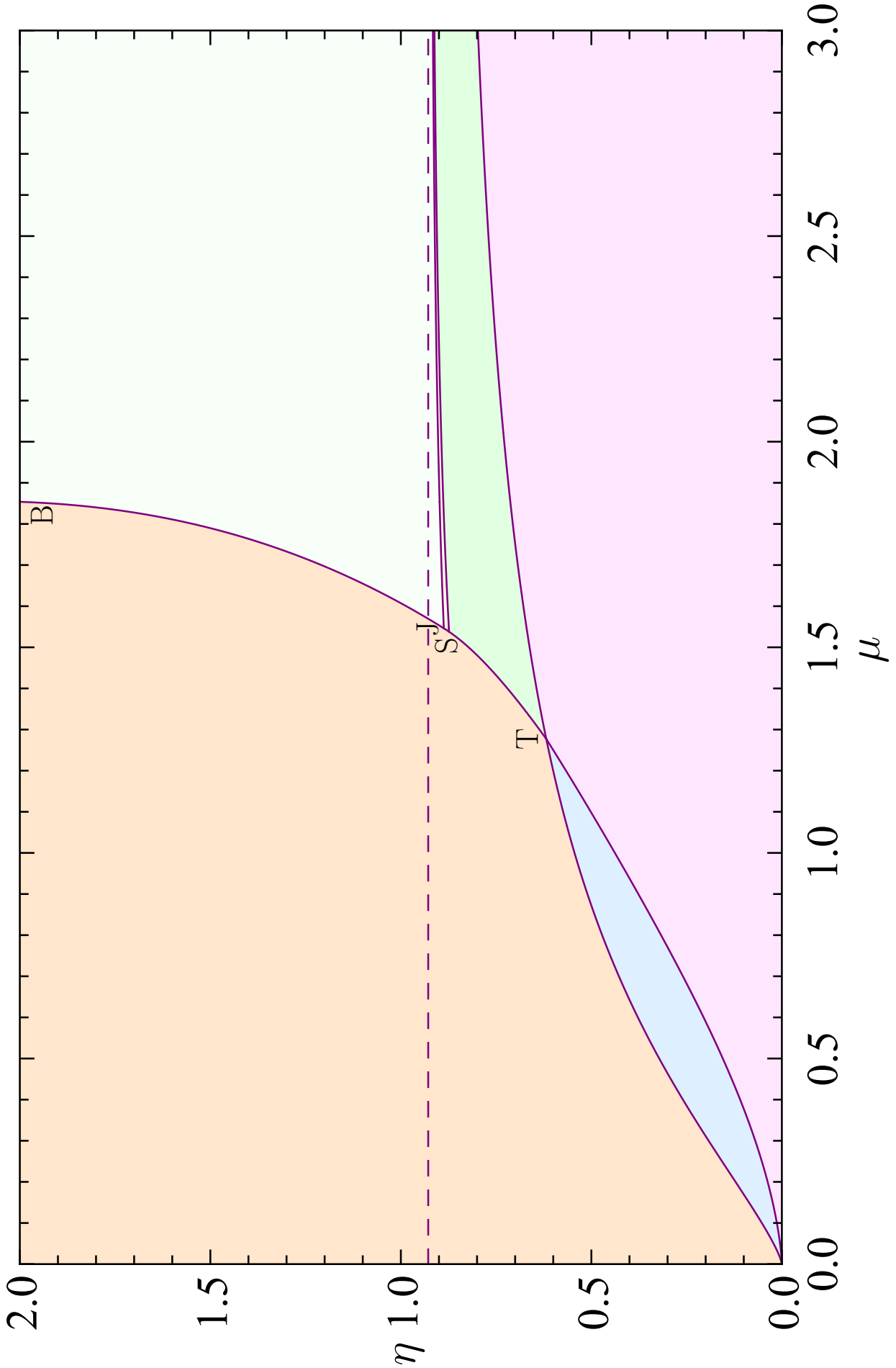

Figure 6: Filled η-μ domains of self-standing and collapse states for M-like distribution.

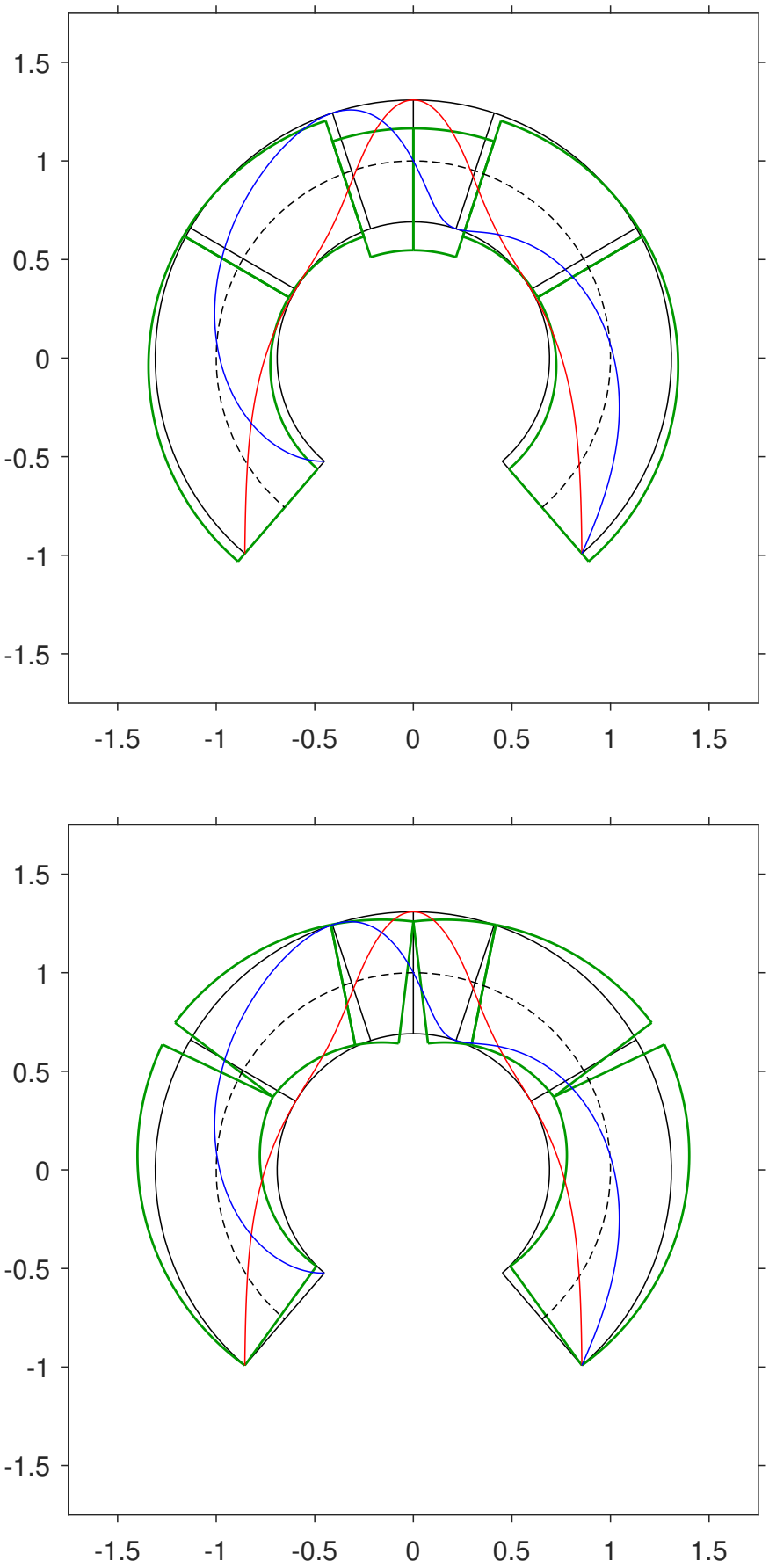

Figure 7: Least-thickness collapse mechanism, with line of thrust and line of friction: at Triple point with $\alpha_T^M = 2.430069103769349 \simeq 139.2°$, $\mu_T^M = 1.277021363435198$ ($\varphi_T^M \simeq 51.9°$), $\eta_T^M = 0.6183182410743238$ ($\beta_r \simeq 59.7°$, $\beta_s \simeq 18.3°$): purely-sliding (top); purely-rotational (low).

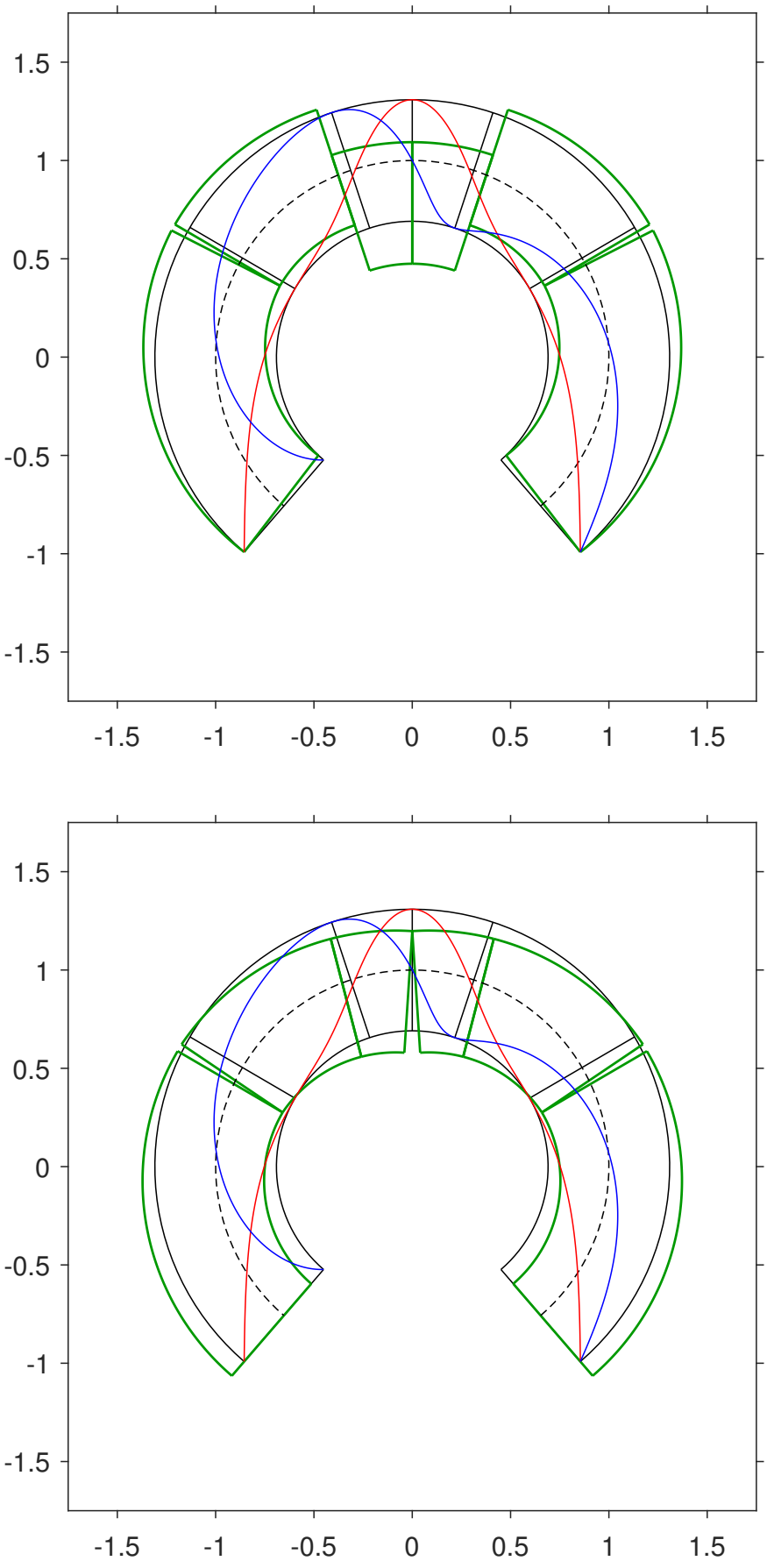

Figure 8: Least-thickness collapse mechanism, with line of thrust and line of friction: at Triple point with $\alpha_T^M = 2.430069103769349 \simeq 139.2°$, $\mu_T^M = 1.277021363435198$ ($\varphi_T^M \simeq 51.9°$), $\eta_T^M = 0.6183182410743238$ ($\beta_r \simeq 59.7°$, $\beta_s \simeq 18.3°$): rotational-sliding (top); sliding-rotat. (low).

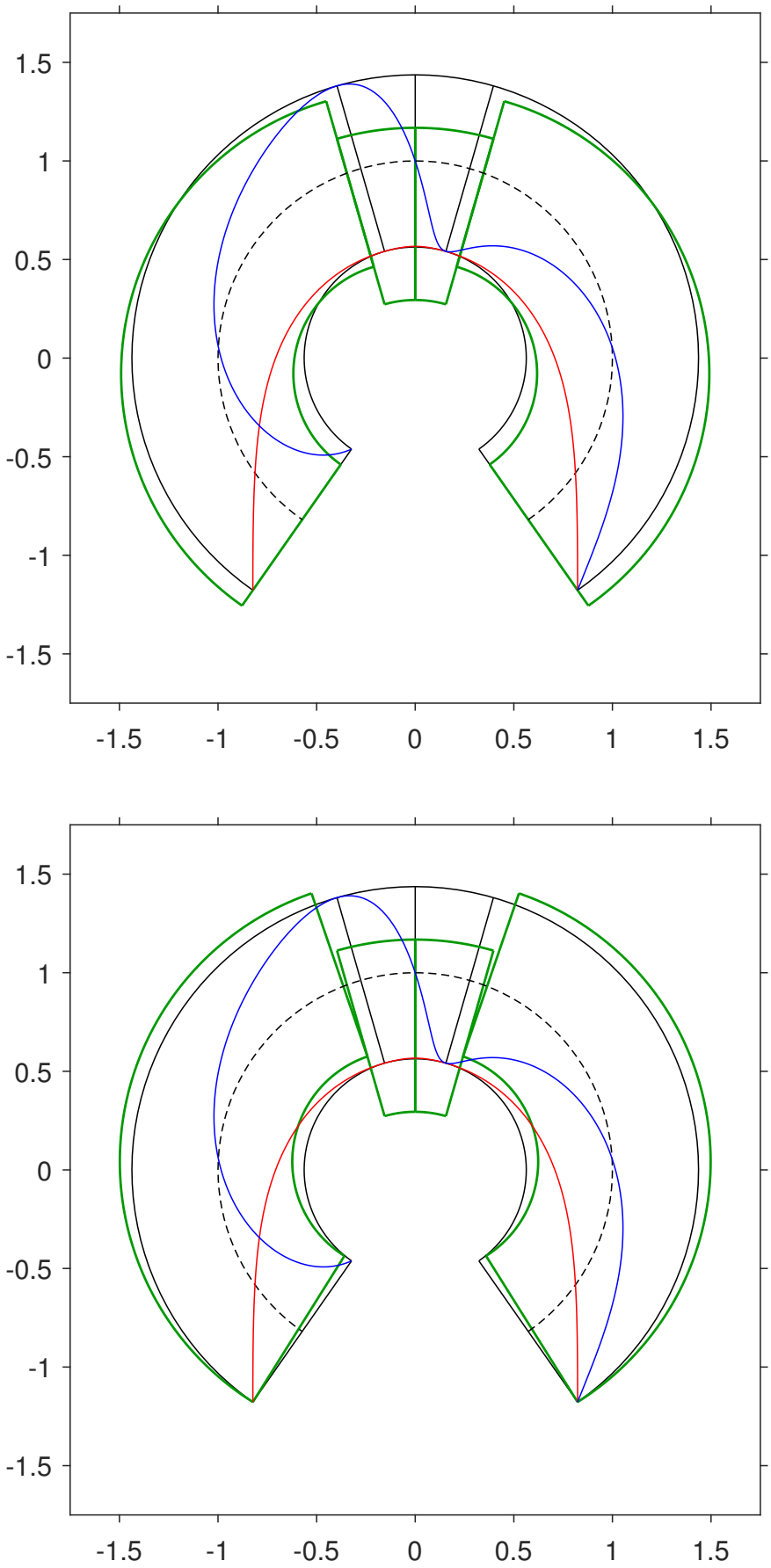

Figure 9: Least-thickness collapse mechanism, with line of thrust and line of friction: at Shift point with $\alpha_S^M = 2.531269027051532 \simeq 145.0°$, $\mu_S^M = 1.537913842804309$ ($\varphi_S^M \simeq 57.0°$), $\eta_S^M = 0.8734660698200912$ ($\beta_r = \beta_s \simeq 16.0°$): purely-sliding (top); rotational-sliding (low).

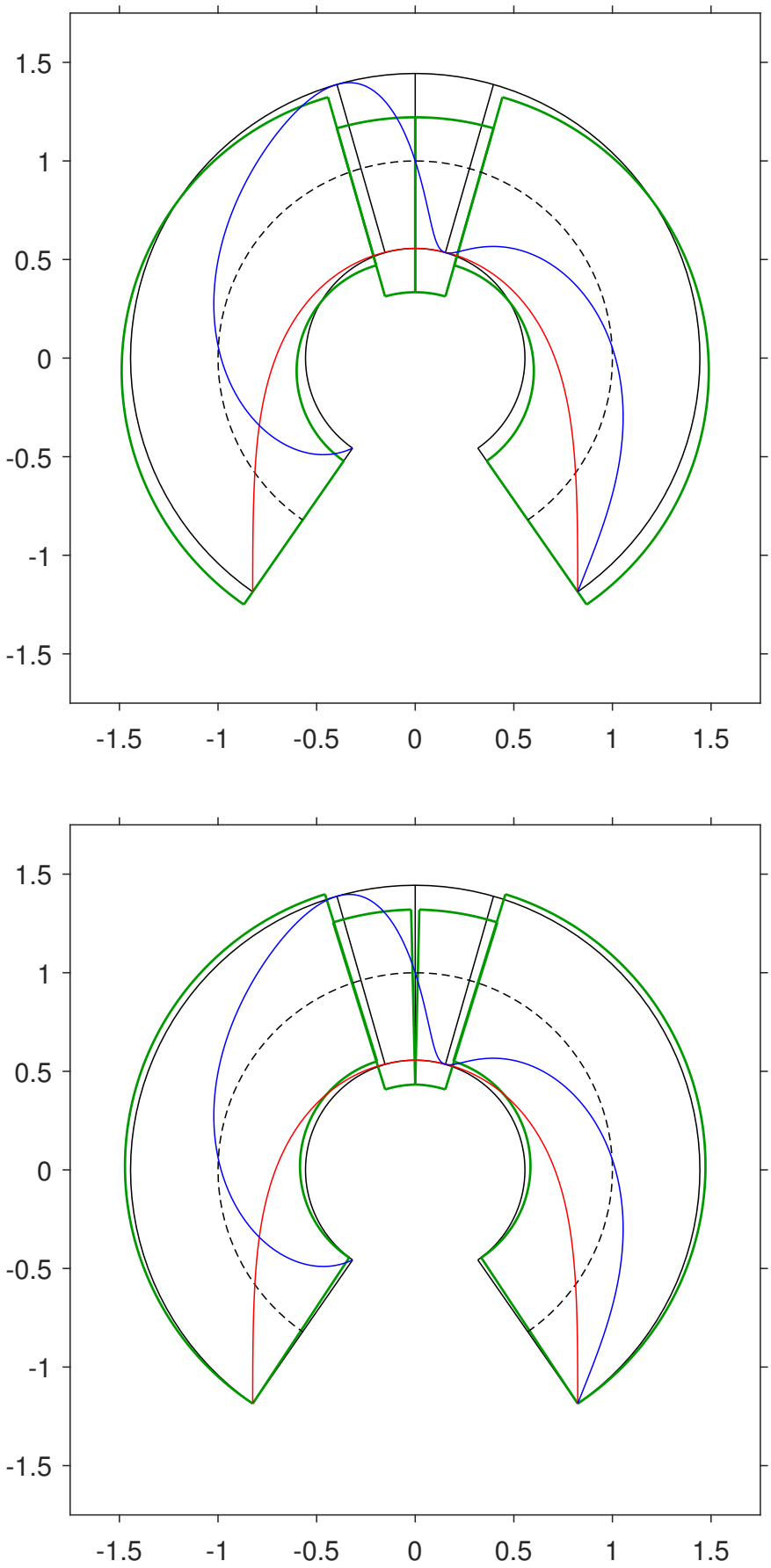

Figure 10: Least-thickness collapse mechanism, with line of thrust and line of friction: at Junct. point with $\alpha_J^M = 2.534077907926732 \simeq 145.2°$, $\mu_J^M = 1.546270800988723$ ($\varphi_J^M \simeq 57.1°$), $\eta_J^M = 0.8872221963291936$ ($\beta_r = 0$, $\beta_s \simeq 16.0°$): purely-sliding (top); rot.(overturn.)-sliding (low).

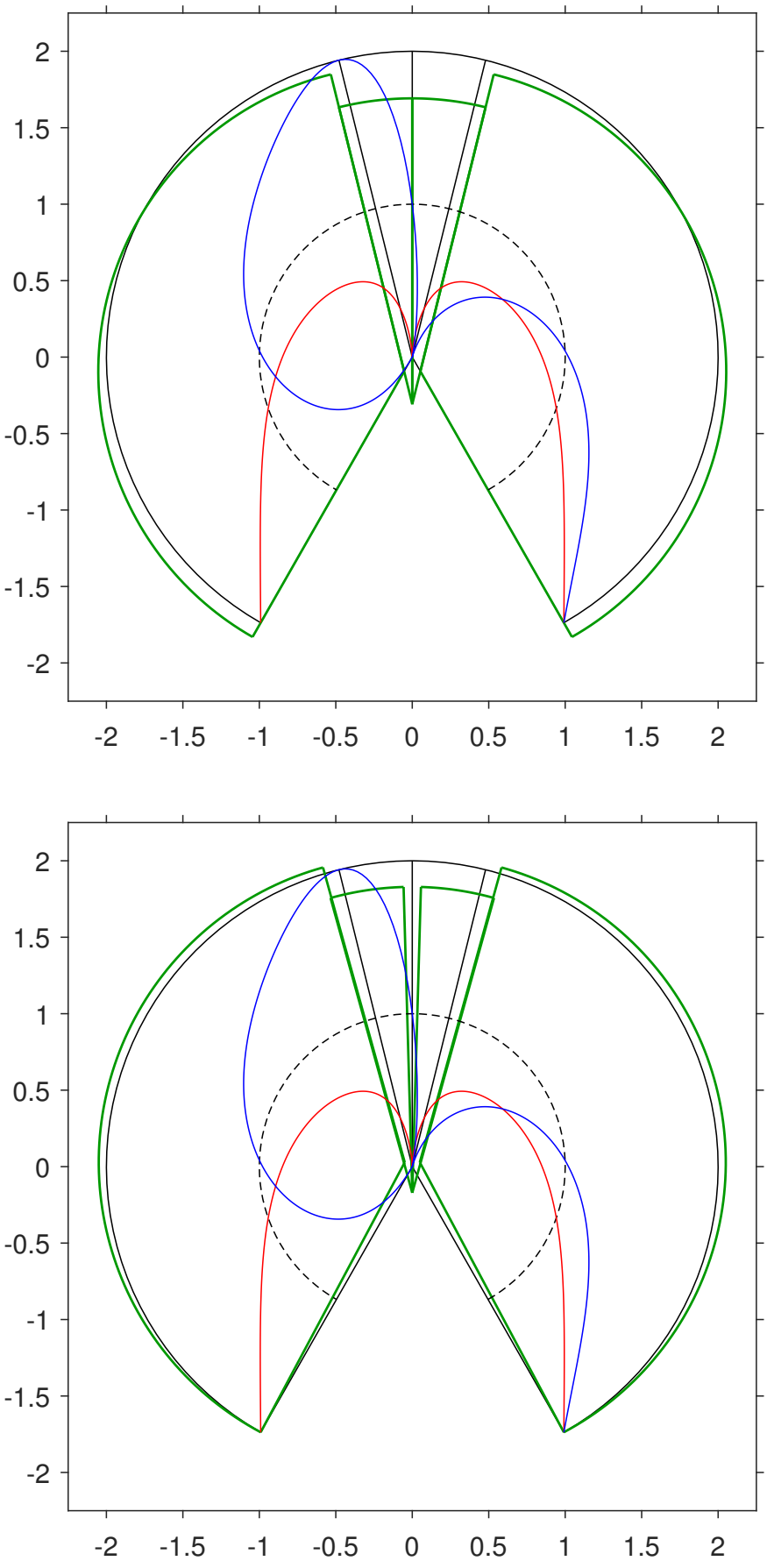

Figure 11: Least-thickness collapse mechanism, with line of thrust and line of friction: at Border point with $\alpha_B^M = 2.623074865083552 \simeq 150.3°$, $\mu_B^M = 1.853774888450581$ ($\varphi_B^M \simeq 61.7°$), $\eta_B = 2$ ($\beta_r = 0$, $\beta_s \simeq 13.9°$): purely-sliding (top); overturning-sliding (low).

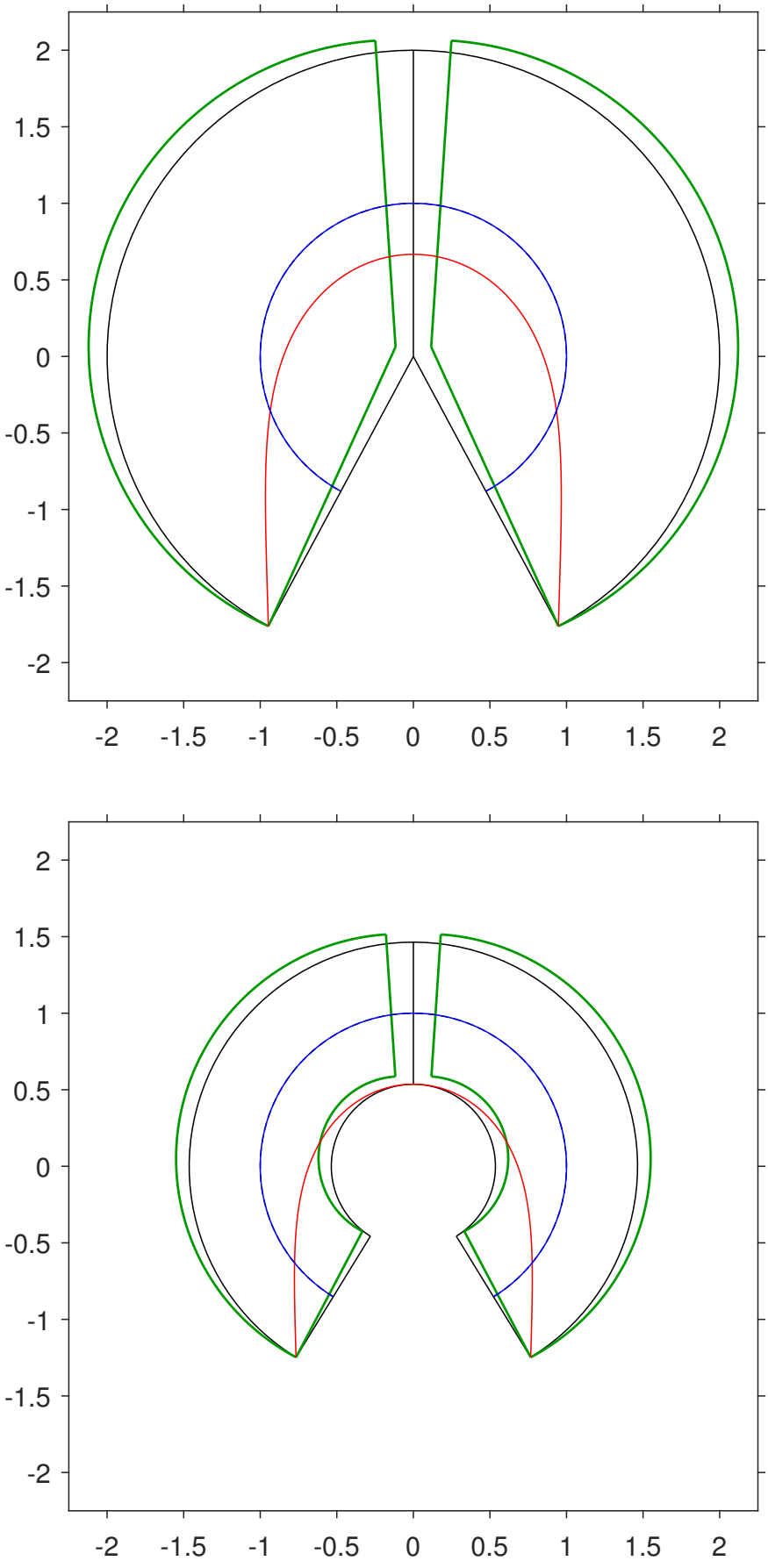

Figure 12: Least-thickness collapse mechanism, with line of thrust and line of friction: purely-overturning at $\mu\to\infty$ (φ=90°): $\alpha_L^M = 2.648388899151005 \simeq 151.7°$ ($A_L^M = 2/3$), $\eta_L = 2$ (top); $\alpha_l^M = 2.590843443008955 \simeq 148.4°$ ($A_l^M = \sqrt{3} - 1$), $\eta_l^M = 2(2\sqrt{3} - 3) \simeq 0.93$ (low).